The Dissertation Committee for Lynn June Rozanski Certifies that this is the approved version of the following dissertation:

Studies on Conjugated Polymer Thin Film Morphology: Effect on Emission and Charge Transport

Committee:

David A. Vanden Bout, Supervisor

Paul F. Barbara

Keith J. Stevenson

Richard M. Crooks

John W. Keto

Studies of Conjugated Polymer Thin Film Morphology: Effect on Emission and Charge Transport

by

Lynn June Rozanski, B. S.

Dissertation

Presented to the Faculty of the Graduate School of

The University of Texas at Austin

in Partial Fulfillment

of the Requirements

for the Degree of

Doctor of Philosophy

The University of Texas at Austin

May 2007

Dedication

For Margy Hougland and Richard Rozanski.

For supporting my dreams and hopes, and providing guidance whenever I needed it.

Thanks, Mom and Dad.

Studies of Conjugated Polymer Thin Film Morphology: effect on Emission and Charge Transport

Publication No._____

Lynn June Rozanski, Ph. D.

The University of Texas at Austin, 2007

Supervisor: David A. Vanden Bout

Since their discovery, semiconducting conjugated polymers have shown great promise as active materials for a range of electronic devices. Initially desired for their high quantum yield, conjugated polymers have become popular due to their low cost and potential to be transferred to existing technology. Conjugated polymers are liquid crystalline, packing into well ordered domains upon thermal annealing of the films, which often leads to complex polymer interactions that can affect their semiconducting properties such as charge transport, emission color and ultimately device efficiency. Film morphology is difficult to characterize, with the order often varying on the nanoscale within a film. Near field scanning optical microscopy (NSOM) combined with Atomic Force Microscopy (AFM) can probe the degree of order of a film on the nanoscale and correlate it to topography; this can then be related to changes in luminescence emission and device characteristics to infer how

charges are moving within a film. The effect of morphology on device function can vary between polymer systems; for example, di-alkyl polyfluorenes (PFs), a popular blue emitter for LEDs, undergo fluorescence degradation from ketone-based defects. Ordering of PF films containing some chemical defects increased the energy transfer from pristine chains to defects, increasing the defects' degrading effect on the film emission. In comparison, the air-stable di-alkyl polyphenylene ethynylenes (PPEs) have numerous chain interactions in the amorphous pristine film, but show evidence of fewer interactions between these chains after ordering the film rather than more interactions. PPE polymers with varied lengths of sidechains produce dissimilar electroluminescence intensities, due to differences in their morphologies that affected how charges moved and recombined within the films. Understanding the effect of changes in polymer film morphology on luminescence and charge movement will help future efforts in understanding more complex polymer interactions, such as seen in blended polymer films.

Table of Contents

List of Figures

CHAPTER 1: INTRODUCTION TO CONJUGATED POLYMERS AND SCANNING METHODS FOR THIN FILMS

DISSERTATION OVERVIEW

Chapter 1 covers the background of conjugated polymers and their use in optoelectronic devices, along with the tools for examining them such as NSOM and AFM. These semiconducting conjugated polymers (CPs) have shown considerable promise as inexpensive alternatives to inorganic-based active materials in optoelectronic devices. All conjugated polymers contain rigid, often aromatic backbones, coupled with alkyl sidechains to increase solubility, and the ability to work with these polymers in solution allows for them to be applied over large-area, flexible substrates. Since conjugated polymers are often liquid crystalline, they have a range of complex interactions when spincast into films, and these interactions between polymer chains or within individual chains can affect charge transport and emission color; ultimately determining how a device functions. There are currently few means to measure order on a molecular size scale, but changes in the film topography can be monitored on the nanoscale using the scanning probe technique Atomic Force Microscopy (AFM). Film fluorescence emission can also be probed on the nanoscale using Near-field Scanning Optical Microscopy (NSOM), providing information on the chain order within the film in relation to its topography. An introduction to conjugated polymers, light emitting device basics, and the high resolution scanning probe techniques of NSOM and AFM are in Chapter 1.

Chapter 2 covers in depth the studies on di-alkyl polyfluorenes, initially covering previous research, which indicated that the amount of green emission seen for films was related to the degree of their order. This unwanted green emission was initially believed to be from aggregates, then evidence for chemical defects was seen in IR spectra of films, identified by others as the sole source of the undesired green emission, implying that interactions between polymer chains was irrelevant, but there was still considerable debate on the exact nature of the source of the green emission. Since the intensities of both the blue emission and the green emission change simultaneously during film treatments, it was necessary to examine film fluorescence changes in situ to allow for a direct comparison of emission spectra as well as to monitor the quantitative changes. In order to see if interchain interactions were necessary for green emission, dilute PF films in an inert matrix of polystyrene or PMMA were photobleached, with results indicating that intrachain energy transfer alone was sufficient. It was possible to prevent defect formation in films annealed under dried argon or nitrogen, as these films did not show an increase in green emission. Thus it was possible to monitor the changes in emission for films containing a small number of defects, proof that the increased packing order of the film led to more efficient energy transfer to the few defect sites within the film, resulting in an increased green emission. Various control experiments were also conducted to ensure that the degree of order was the vital parameter in increasing the green emission seen for the annealed films already containing a few defects.

Chapter 3 includes studies performed on polyphenylene ethynylene-based light emitting devices. Previous work that had focused on the film fluorescence of the long sidechain DPPE is included as it relates to both the electroluminescence of devices as well as for comparison with the shorter sidechain NPPE. The two polymers have identical fluorescence spectra- structured blue emission in dilute solution, a broad green

fluorescence in the pristine film, and a blue-shifted, structured fluorescence seen in the annealed film. Comparison of the electroluminescence between the two polymers reveals some slight differences, with the DPPE LEDs producing a broad green excimer-based emission in both the pristine and annealed LEDs, while the NPPE LEDs have a larger difference between the EL spectra collected for the pristine and annealed devices. The annealed NPPE EL has more of the blue-shifted and structured emission, but also contains a fair amount of the excimer-based emission. Due to the identical fluorescence behavior between the two polymers, only differences in the their respective morphologies can account for the differences in their respective EL spectra, and since the NPPE LEDs had less of the excimer-based emission in the annealed state, it was plausible that the shorter side-chain films ordered to a greater degree than the longer sidechain DPPE. However, NSOM polarization studies revealed that the NPPE films ordered to a lesser degree than the DPPE, so the morphology differences between the two films cannot be seen at this resolution. Also, since the annealed EL in DPPE is dominated by the few excimer sites still remaining within the film, these devices had decreased light emission intensities compared to the pristine devices, and did not produce EL nearly as often. The EL in the annealed NPPE, dominated to a lesser degree by the green excimer emission, functioned considerably better than the annealed DPPE devices.

Chapter 4 is a technical chapter covering the production and testing of the sandwich LEDs used in Chapter 3. There are many setbacks towards the production of working devices, and a large amount of research has focused on methods to improve charge injection and transport within devices for efficiency. Simply following another's technique in order to make a working device is insufficient; there are currently no standard production methods. A general trend in increasing efficiency in a device is to use plasma treatments of the ITO anode (with multiple debates over which treatment

provides the best result), as well as coat the anode with a thin layer of hole-transport material such as PEDOT-PSS. Testing of various ITO treatments found that oxygen plasma cleaning of the ITO anode led to the best device performance; while inclusion of the hole transport material PEDOT-PSS led to longer device lifetime, but no change in turn on voltage. Inclusion of a thin insulating layer NaOH before application of the cathode helped produce a brighter device, but controlling the thickness of this layer (~1-2 nm) hindered further testing. Ultimately the device performance depended on a number of parameters: lowering the injection barrier of carriers into the film was essential, switching to smaller active areas helped to produce more working devices, while the inclusion of various transport layers merely tweaked device performance rather than having a significant effect on whether the device worked or not, indicating that optimization of preparation techniques is necessary for the best device performance.

.

CONJUGATED SEMICONDUCTING POLYMERS USED IN LEDS AND PHOTOVOLTAICS

Since the discovery of electrically conductive polymers by Heeger, MacDiarmid, and Shirakawa,[1] numerous semiconducting conjugated polymers have been synthesized for use over a range of electronic devices, from LEDs[2-6] and transistors,[7,8] to photovoltaics.[9-11] One reason conjugated polymers (CPs) are appealing as active materials for light emitting devices is that they can be chemically tailored to emit at a desired wavelength; CPs are also solution processable, allowing for a possible transfer to existing roll-to-roll technologies as well as the ability to be applied to flexible substrates, providing an inexpensive alternative to inorganic-based active materials. However, once these polymers are spincast as films, the complex interactions between polymer chains can have a dramatic effect on the emission color.[12-15] In addition to spectral shifts, these interactions have also been shown to affect the intensity of luminescence and the degree

of charge transport within films, ultimately affecting device efficiency.[12,14-15] It is not sufficient to simply remove interchain interactions altogether, as the increased order contributes to increased charge transport within the film,[12,15] thus finding an optimal balance between charge transport and luminescence is a necessity. For the future production of efficient polymer light emitting devices (PLEDs), it is important to understand the morphology of the film on the nanoscale and how it relates to emission, charge transport, and device function. A solid understanding of how charge transport is affected by film morphology in these films could contribute to understanding more complex interactions in novel polymer systems, such as the mixed polymer films used in solar cells.[16-17] The morphology in these films can be probed through high-resolution scanning techniques such as Near field Scanning Optical Microscopy (NSOM) and Atomic Force Microscopy (AFM), providing information on how the polymers are aligned and to what degree they order,[18-19] which then is related to their emission and function in devices.

SEMICONDUCTING CONJUGATED POLYMERS

The highly fluorescent polymers used in optoelectronic devices contain rigid ring systems along their polymer backbones; this conjugation allows the extended p_z orbitals to overlap, producing a delocalized -electron cloud along the backbone; an example of this delocalization is shown in Figure 1.1, illustrating delocalization in the polyphenylene ethynylene backbone. The electron cloud delocalization extends along the length of the polymer chain and facilitates the movement of charges along the polymer backbone or between close neighboring polymer chains, giving the polymer its semiconducting property.

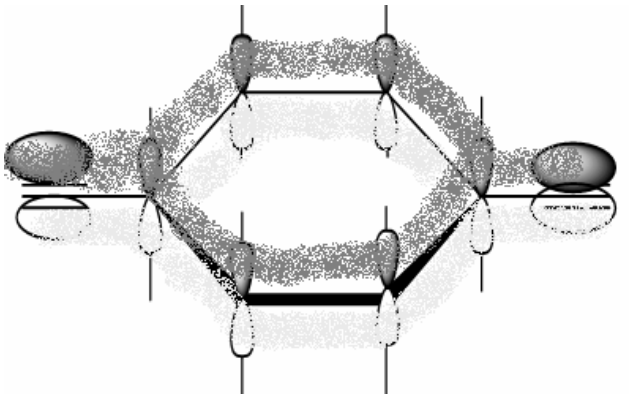

Figure 1.1 Depiction of the p_z orbitals in the structure of PPE, showing the delocalization of the -electron cloud.

Various sidechains are incorporated off of the backbone to increase solubility of the polymer in common solvents. While the sidechains themselves do not contribute to the color of emission, they can lead to increased interactions between polymer chains, affecting device emission and efficiency.[20-21] The structures of two types of conjugated polymers used in this study, which show great promise as active materials in optoelectronic devices, are di-alkyl polyfluorene and di-alkyl polyphenylene ethynylene, shown respectively in Figure 1.2.

In conjugated polymers, the overlap of multiple highest occupied molecular orbitals (HOMOs) and multiple lowest unoccupied molecular orbitals (LUMOs) behave in a manner analogous to the valence and conduction bands, respectively, of inorganic semiconductors, and similar to their inorganic counterparts they can be effectively used as an active material in optoelectronic devices. Highly fluorescent, various conjugated polymers have been able to produce devices with high external quantum efficincies.[22,23]

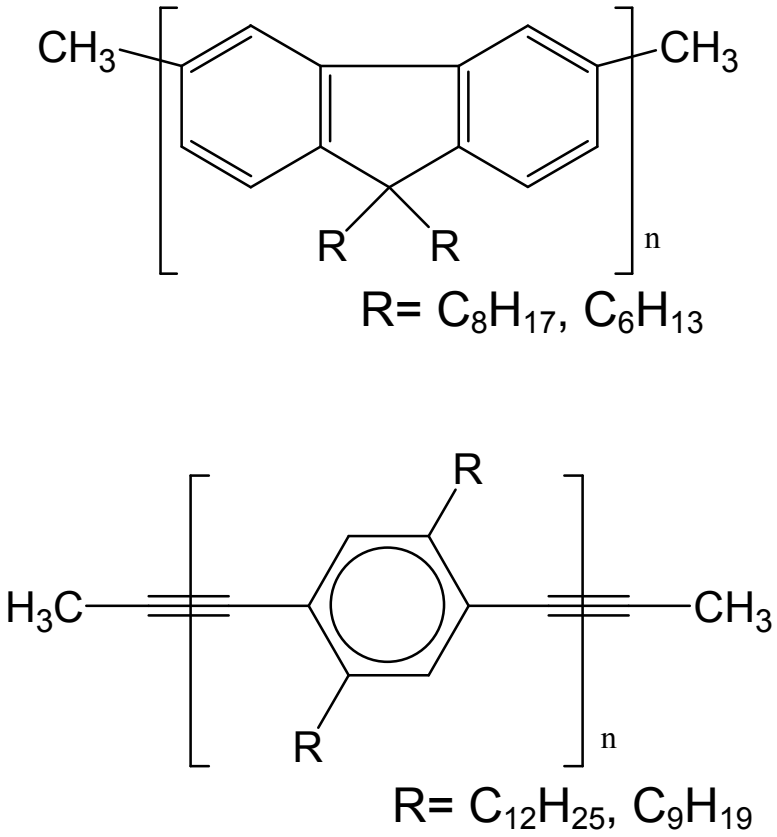

Figure 1.2 Structures of the conjugated polymers Dialkyl Polyfluorene (top), and Dialkyl polyphenylene ethynylene (bottom), showing their rigid, conjugated polymer backbones. Polymers with varied lengths of the straight alkyl sidechains (R), were examined.

POLYMERS IN OPTOELECTRONIC DEVICES

The basic configuration of a simple optoelectronic device is applicable to both light emitting devices (LEDs) and photovoltaics (PVs); the setup used for the PPE-based LEDs examined is shown in Figure 1.3. In a simple polymer LED, the polymer film is sandwiched between two electrodes, usually spincast from solution to produce a ~100 nm

thick film; the electrodes are chosen so that they have a good match of their workfunctions to the HOMO and LUMO levels of the polymer used, increasing the charge injection into the polymer film.[24] The anode most commonly used in these devices is made from indium tin oxide (ITO) films on glass substrates. ITO has a relatively high workfunction (~ 4.5 eV),[24] making it viable as a material for hole injection, and it has a good optical transparency, allowing the electroluminescence produced by the polymer to leave the device. Most conjugated polymers are hole-transport materials, having very low LUMO levels; thus lower workfunction metals such as calcium or magnesium, capped by a protective thin layer of aluminum, are used as the anode for efficient electron injection[24]; although the few electron-transport polymers generally use the higher workfunction metals aluminum or silver as the device cathode.

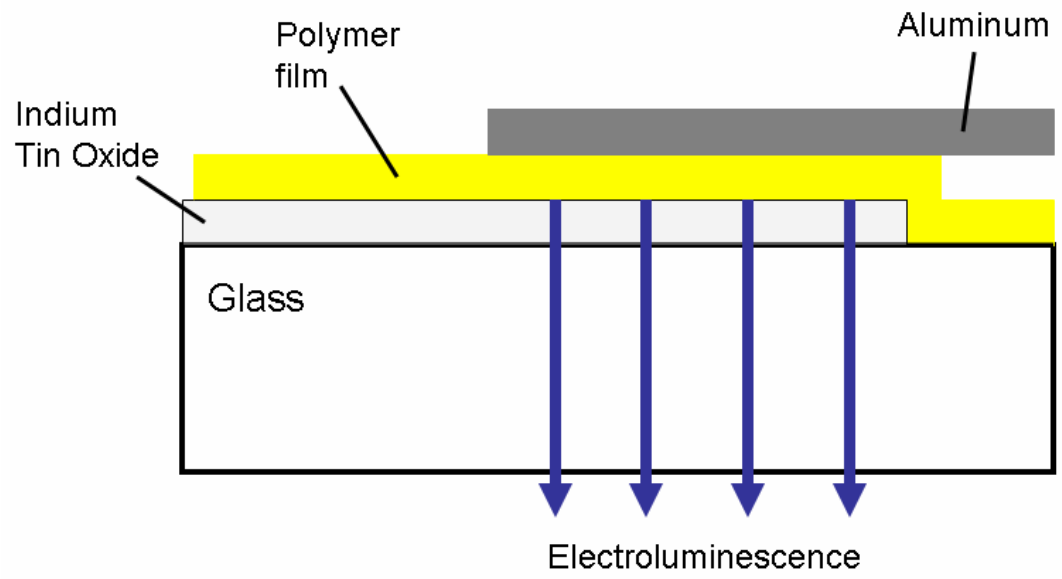

Figure 1.3 Light emitting device schematic for the PPE polymer LEDs.

The production of efficient polymer LEDs depends on a number of factors, including: the amount of charges injected into the polymer film from each electrode, the mobility of these charges through the film, the recombination efficiency of these charges within the polymer film. It is rare for the workfunction of the electrodes to be closely matched to the HOMO and LUMO levels of the polymer, thus attempts are made to change the workfunction of the materials, or to increase the tunneling of charges through the energy barrier. Increased hole injection from the ITO anode is often performed in two different ways: lowering the workfunction of the ITO through plasma treatments, and/or including another polymer layer with an even lower workfunction than the ITO itself, such as poly(3,4-ethylenedioxythiophene) polystyrenesulfonate, (PEDOT-PSS), which has a workfunction of ~ 5 eV, lower than ITO's 4.5 eV workfunction.[25] Injection improvements from the cathode have been seen when a very thin layer of insulating material such as lithium fluoride (LiF) has been included between the polymer and the metal cathode, although the exact method of how this layer improves the charge injection is under some debate.

The morphology of the conjugated polymer film can also have a dramatic effect on the function of a LED, since interactions between polymer chains can lead to changes in the film's emission and charge transport properties. There are two types of undesired interactions between polymer chains: aggregates and excimers. The formation of the aggregated species, defined as either a physical agglomeration of polymer chains, or ground-state electronic interactions between chains, leads to spectral changes in both the absorption spectra and emission spectra of a polymer film. Excimers are excited-state electronic interactions between polymer chains, and are evidenced as only changes in the film's fluorescence emission. It is not unusual to see evidence for either of these interchain interactions in conjugated polymers popular for use in LEDs; excimer

emission has already been shown for one of the polymers in this study, Di-dodecyl poly(phenylene) ethynylene (DPPE).[26]

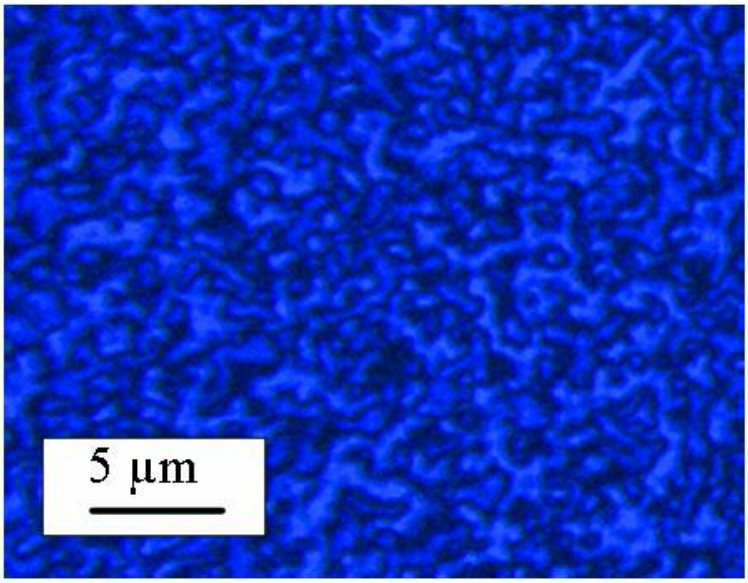

Figure 1.4 Polarized optical micrograph of an annealed DPPE film, showing the micron-sized ordered domains.

Both of the polymers used in this study are liquid crystalline polymers, with the polymer chains aligning and packing together into domains upon thermal annealing. Straight alkyl sidechains allow for a close packing order of the polymer chains, often increasing the interactions between them. One of the easiest methods to see evidence of this increased packing order is by placing the annealed polymer film between crossed polarizers on a microscope. The aligned polymer chains within the domains polarize the light passing through the film, showing up as birefringence, an example of which is shown in Figure 1.4, for an annealed DPPE film. It is also possible to essentially zoom

in on these ordered domains and examine them on the nanoscale using scanning probe techniques such as Near field Scanning Optical Microscopy (NSOM) and Atomic Force Microscopy (AFM).

HIGH RESOLUTION SCANNING PROBE METHODS

Conventional microscopy, which was used to produce the image seen in Figure 1.4, has its resolution limited by the wavelength of light used to illuminate the sample, with resolution approximately half the wavelength of light used, /2; in the visible range, this means a resolution limit around 200-300 nm. Near field Scanning Optical Microscopy (NSOM) is a technique with lateral imaging resolution on size scales considerably smaller than far-field microscopy. A diagram illustrating the NSOM setup is shown in Figure 1.5. NSOM uses a fiber optic that has been pulled down to a fine taper, producing an aperture at the tip between 50- 150 nm in diameter. The tapered part of the fiber optic is then coated with highly reflective aluminum- as the pulled portion of the fiber has lost its total internal reflection capability; a SEM image of a NSOM tip is shown in Figure 1.6. Laser light is fed into the fiber optic, and reflected down to the aperture of the tip, which is then maintained in the near-field of the sample, approximately 5-10 nm from the sample surface. In the near-field, the light from the NSOM tip is localized on its surface, producing an evanescent wave that is then used to excite the polymer film directly beneath it.

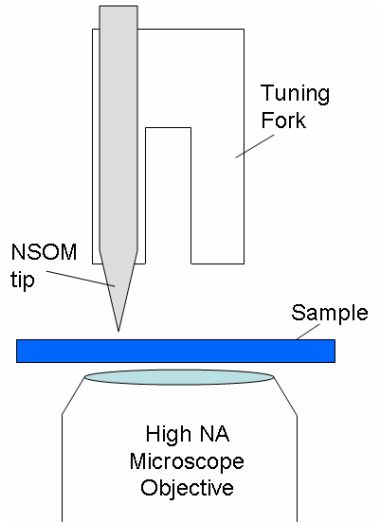

Figure 1.5 Diagram of the NSOM setup, showing the NSOM tip, oscillated by the tuning fork; damping of the oscillations is monitored to keep the tip at a set distance. Emission from the sample is collected through a microscope objective and sent to detectors.

Within the near-field, the image resolution is no longer defined by the wavelength of light used, instead it depends only on the size of the tip aperture; the small aperture size of the NSOM tips allows for this increased lateral resolution. The tip is attached to a tuning fork to oscillate it at its resonate frequency; the damping of the oscillation signal as the tip approaches the surface is monitored; allowing for both the desired distance between the sample surface and tip to be maintained, as well as changes in the topography to be measured. Since the tip is raster-scanned over the sample surface, film topography and optical information are obtained simultaneously, allowing for the optical image to be directly related to the film morphology. Light emission from the polymer films is collected through a microscope objective placed beneath the film, then directed to one or more detectors. In order to determine the degree of order within annealed polymer films, the fluorescence emission collected from the film passes through a polarizing beam

splitter and is sent to two different detectors, monitoring the emission polarized orthogonal and parallel to the scanning direction. These are referred to as the x (vertical) and y (horizontal) polarizations, respectively, and allow for the calculation of anisotropy within the film, showing the alignment of polymer chains as well as the percentage of polymer aligned in the domains.

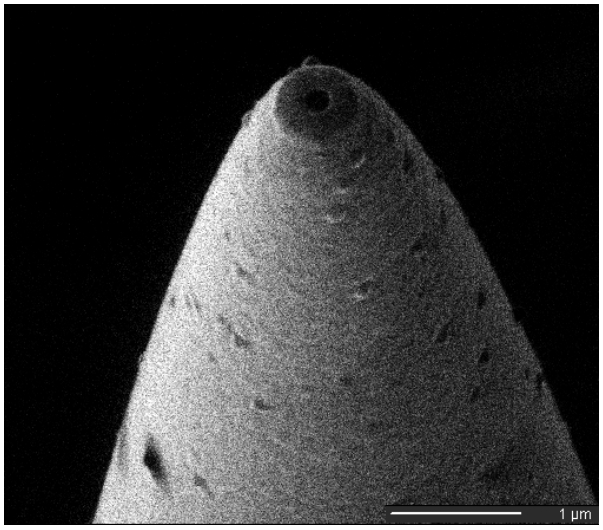

Figure 1.6 SEM image of NSOM tip, showing the small aperture and aluminum coating.

Atomic Force Microscopy (AFM) provides a higher degree of lateral resolution compared to NSOM, but does not provide any optical information, making the two techniques complementary. Due to the large size of the entire NSOM tip (seen in Figure 1.6), the fine variations in topography are often beneath its resolution. Thus the higher-resolution topographies provided by AFM illustrate the finer details lost in the NSOM topography scans, and can be correlated to the finer optical detail in NSOM fluorescence images. AFM uses a sharp (~20 nm), hard silicon nitride probe attached to a cantilever, which in these studies was used in tapping mode, where the cantilever was oscillated at

its resonate frequency (similar to NSOM), and placed close enough to the sample surface that the tip intermittently makes contact with the surface, this technique is nondamaging to the surface. A laser beam is bounced off the end of the cantilever, and centered onto a split photodiode, this is diagrammed in Figure 1.7. When the tip is deflected, the movement of the reflected laser beam is monitored on the photodiode and related to the topography of the sample. Numerous examples of AFM topography scans are shown in both Chapters 3 and 4.

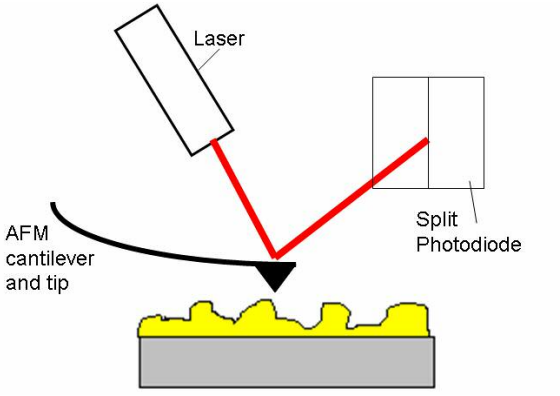

Figure 1.7 Diagram of AFM setup, illustrating the silicon nitride tip and laser beam reflected from the tip onto a split photodiode. Tip deflection is monitored by changes of laser beam position on the photodiode.

CHAPTER SUMMARY

Interest in conjugated polymers as active materials in optoelectronic devices has increased dramatically since their discovery due to the fact that they provide an inexpensive alternative to traditional inorganic semiconductor technology. However, polymer devices do not perform nearly as well as their inorganic and small molecule counterparts, due to intermolecular interactions and problems with charge transport and

charge injection into these films. The complex interactions between polymer chains in thin films are still not completely understood, and due to their effect on how the polymer film will function in a device, it is important to study the relation between polymer morphology and its effect on properties such as charge transport and film emission. A good foundation of the principle effects of interchain interactions and charge transport within a simple polymer film can help understanding of more complex processes occurring in novel and poorly understood polymer systems- such as mixed polymer photovoltaics.

REFERENCES

1. H. Shirakawa, E. J. Louis, A. G. MacDiarmid, C. K. Chiang and A. J. Heeger, *J. Chem. Soc. Chem. Comm.* **1977**, 579.

2. J. H. Burroughes, D. D. C. Bradley, A. R. Brown, R. N. Marks, K. Mackay, R. H. Friend, P. L. Burns and A. B. Holmes, *Nature* **1990,** *347,* 539.

3. R. H. Friend, R. W. Gymer, A. B. Holmes, J. H. Burroughes, R. N. Marks, C. Taliani, D. D. C. Bradley, D. A. Dos Santos, J. L. Bredas, M. L. Logdlund, and W. R. Salaneck, *Nature* **1999**, *397*, 121.

4. F. Huang. H. Wu, D. Wang, W. Yang, and Y. Cao, *Chem. Mat.* **2004**, *16*, 708.

5. C-H. Chou, S-L. Hsu, S-W. Yeh, H-S. Wang, and K-H. Wei, *Macromolecules* **2005**, *38*, 9117.

6. C. Schmitz, P. Posch, M. Thelakkat, H-W. Schmidt, A. Montali, K. Feldman, P. Smith, and C. Weder, *Adv. Funct. Mater.* **2001**, *11*, 41.

7. N. Stutzmann, R. H. Friend, and H. Sirringhaus, *Science* **2003**, *299*, 1881.

8. H. Sirringhaus, T. Kawase, R. H. Friend, T. Shimoda, M. Inbasekaran, W. Wu, and E. P. Woo, *Science* **2000**, *290*, 2123.

9. H. J. Snaith, A. C. Arias, A. C. Morteani, C. Silva, and R. H. Friend, *Nano. Lett.* **2002**, *2*, 1353.

10. K. Colladet, S. Fourier, T. J. Cleij, L. Lutsen, J. Gelan, D. Vanderzande, L. H. Nguyen, H. Neugebauer, S. Sariciftci, A. Aguirre, G. Janssen and E. Goovaerts, *Macromolecules* **2007**, *40*, 65.

11. H. Mizukami, T. Umeda, H. Noda, T. Shibata, A. Fujii and M. Ozaki, *J. of Phys. D: Appl. Phys.* **2006***, 39*, 1521.

12. Liu, J.; Guo, T-F. and Yang, Y. *J. Appl. Phys.* **2002**, *91*, 1595.

13. Leger, J. M.; Carter, S. A.; Ruhstaller, B.; Nothofer, H-G.; Scherf, U.; Tillman, H. and Hörhold, H-H. *Phys. Rev. B* **2003**, *68*, 054209.

14. Shi, Y.; Liu, J. and Yang, Y. *J. Appl. Phys.* **2000**, *87*, 4254.

15. Nguyen, T-Q.; Kwong, R. C.; Thompson, M. E. and Schwartz, B. J. *Appl. Phys. Lett.* **2000**, *76*, 2454.

16. Halls, J. J. M.; Arias, A. C.; MacKenzie, J. D.; Wu, W.; Inbasekaran, M.; Woo, E. P. and Friend, R. H. *Adv. Mater.* **2000**, *12*, 498.

17. Coffey, D. C. and Ginger, D. S. *Nature Mat.* **2006**, *5*, 735.

18. J. Teetsov and D. A. Vanden Bout, *Langmuir* **2002**, *18*, 897.

19. Bunz,U.H.F.; Imhof, J.M.; Bly, R.K.; Bangcuyo, C.G.; Rozanski, L.J. and Vanden Bout, D.A. *Macromolecules* **2005**, *38*, 5892-5896.

20. Peng, K-Y.; Chen, S-A.; Fann, W-S.; Chen, S-H. and Su, A-C. *J. Phys. Chem. B* **2005**, *109*, 9368.

21. Chiavarone, L.; Di Terlizzi, M.; Scamarcio, G.; Babudri, F.; Farinola, G. M. and Naso, F. *Appl. Phys. Lett.* **1999**, *75*, 2053.

22. Yang, X.H.; Müller, D.; Neher, D. and Meerholz, K. Adv. Mater. 2006, 18, 948.

23. Wu, F-I.; Shih, P-I.; Tseng, Y-H.; Shu, C-F.; Tung Y-L. and Chi, Y. J. Mater. Chem. 2007, 17, 167.

24. Friend, R. H. Pure Appl. Chem. 2001, 73, 425.

25. Kim, J. S. ; Granstrom, M.; Friend, R. H.; Johannson, N.; Salaneck, W. R.; Daik, R.; Feast, W. J. and Cacialli, F. *J. Appl. Phys.* **1998**, *84*, 6859.

26. Bunz,U.H.F.; Imhof, J.M.; Bly, R.K.; Bangcuyo, C.G.; Rozanski, L.J. and Vanden Bout, D.A. *Macromolecules* **2005**, *38*, 5892.

CHAPTER 2: FILM MORPHOLOGY IN RELATION TO CHEMICAL DEFECTS OF DI-ALKYLPOLYFLUORENES

BACKGROUND

Polyfluorenes (PFs) are one class of rare blue-emitting polymers, making them popular for use as an active material in LEDs. However, it was discovered early on that use of polyfluorenes within devices degraded their pristine blue emission, decreasing the intensity and red-shifting the color towards a green emission.[1-4] Initially, this shift towards a low energy green emission was believed to be caused by polymer aggregates or excimers, which often lead to a red-shifted emission,[5-8] but it was shown by Heeger et al. and others that oxygen-based defects formed within films with the degraded emission.[9-13] Evidence of these defects was seen in IR spectra of films by the formation of a new peak in damaged films, identified as a cyclic ketone formed along the polymer backbone in place of the alkyl sidechains. Others have created synthetic fluorene/fluorenone copolymers with fluorescence emission identical to that of degraded films, further proof that defects relate to the green emission.[14-16]

The exact relation between these ketone defects and green emission remains under debate, with a new theory put forth by Sims et al.: that ketone defects alone are not sufficient to produce green emission, but rather excimers formed between multiple ketones provide the red-shift in fluorescence.[17] This idea ignited a fresh debate over the relation between defects and film emission, with many papers devoted to disproving the ketone-excimer theory. Single molecule studies and examination of model fluorene/fluorenone oligomers have refuted the ketone-excimer theory, demonstrating

that a single defect in the presence of pristine chromophores was sufficient to produce green emission.[18-21] The majority of these papers have focused on intramolecular interactions between pristine chromophores and defects. The importance of intermolecular interactions should not be disregarded, however, as other papers have claimed intermolecular interactions are necessary for green emission, through studies on the photodegredation of polyfluorene isolated between nanoparticles, and evidence that crosslinked polymers led to a green emission peak distinct from the peak assigned to the fluorene/fluorenone copolymer.[22-23]

A complete understanding of the relation between green emission, morphology and energy transfer within the film is complicated due to a lack of quantification methods for the green emission. Comparisons between different emission spectra are generally done by comparing a ratio of the green peak intensity to the strongest blue peak intensity, and since these peaks change simultaneously during degradation, this ratio can be misleading. A preferable method of quantifying green emission would be to compare the absolute intensities of the blue and green peaks in addition to examining this ratio, thus the absolute changes in emission spectra would indicate how energy transfer is affected by morphology in relation to these chemical defects.

PREVIOUS STUDIES ON POLYFLUORENE, ORDER AND GREEN EMISSION

Previous studies on di-alkyl polyfluorenes used a combination of NSOM and AFM probe techniques to investigate the degree of polymer ordering upon thermal annealing thin films of PFs with varying sidechain lengths.[24-27] The PFs studied had straight alkyl sidechains of either hexyl (PFH), octyl (PFO), or dodecyl carbon chain lengths. All three had different degrees of order after thermal annealing treatments; increased order was seen as the side-chain length decreased, with the

poly(dihexylfluorene) showing the largest degree of order.[24] The examined films had been annealed in an inert argon environment, with fluorescence spectra taken before and after the thermal annealing. A small increase in green emission was seen for the longer sidechain poly(dioctylfluorene), while a large increase in green emission was seen for the short sidechain poly(dihexylfluorene), apparently corresponding to their relative degrees of order. This led to the conclusion that the increased interchain interactions in the shortest sidechain polymer created the most aggregated green emission. Although there were no evidence for defects in the films, it is possible that oxygen or water vapor was not completely removed from the system, and that defects could have been formed through the thermal annealing.

FTIR STUDIES ON POLYFLUORENE FILMS, EVIDENCE OF DEFECTS

FTIR spectra were acquired for poly(dioctylfluorene) and poly(dihexylfluorene) on aluminum or gold-coated silica wafer using a grazing angle configuration. FTIR spectra are shown in Figure 2.1 for a pristine polyfluorene film and a film that has been photobleached beneath a UV lamp for one hour. The two spectra are identical except for the formation of a new peak in the photobleached film at ~1720 cm^{-1}, in the range for a cyclic ketone, as has been reported by others.[9,10] The ketone peak in the photobleached film is indicated by an arrow in graph A. This is the peak that was identified as the ketone defect in damaged films, believed to be the source of green emission. This same ketone peak can be seen in films annealed in air for two hours, but it is a considerably weaker stretch in the thermally annealed film, indicating that fewer defects are formed thermally than through photooxidation. A comparison between the two ketone peaks, illustrating the larger intensity for the photobleached film, is shown graph B of Figure 2.1; the rest of the FTIR spectrum matches that of the pristine and is not shown.

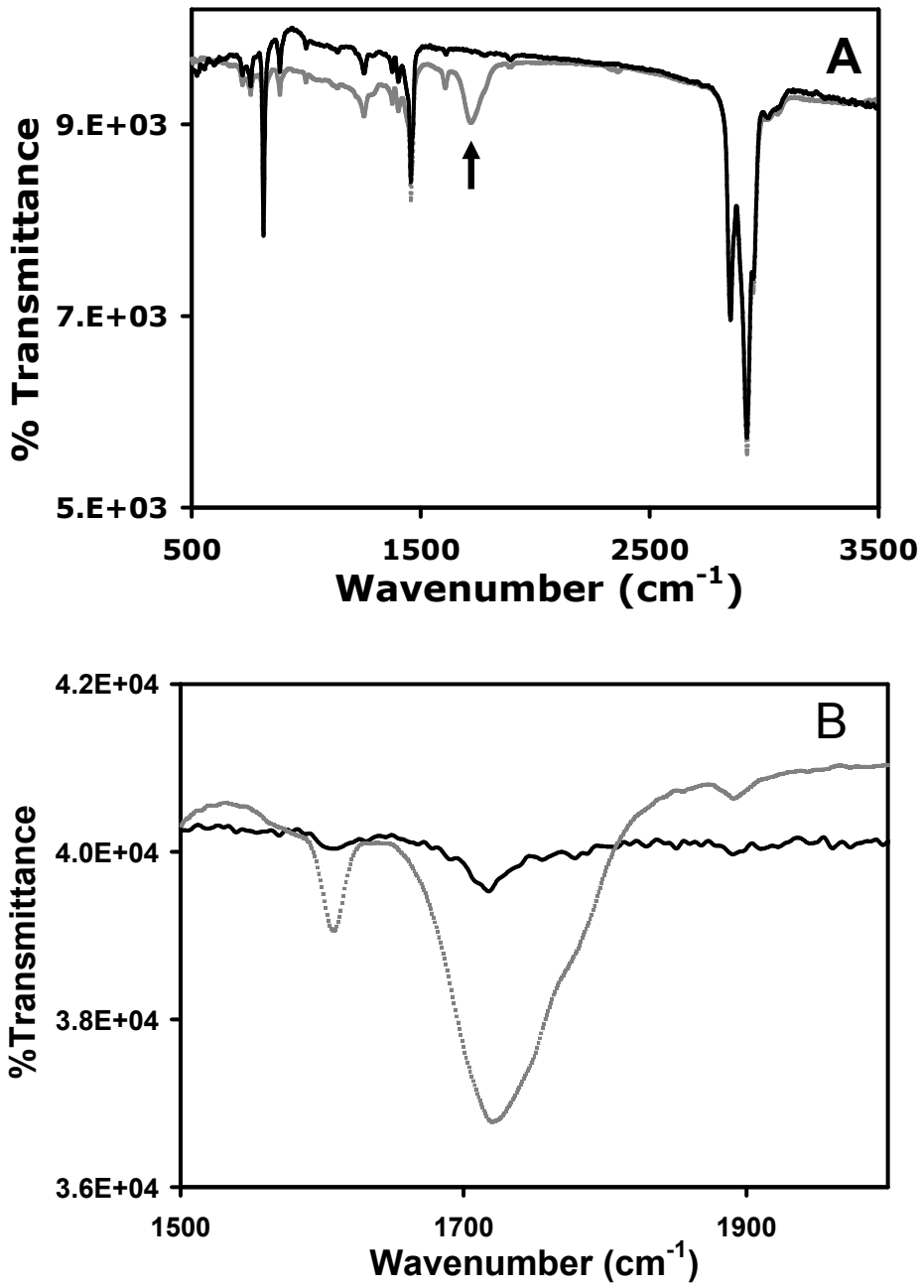

Figure 2.1 Graph A: FTIR spectra for a pristine PFO film (black solid line), and for a photobleached film (grey dotted line). Graph B: FTIR spectra comparing the carbonyl stretch for an air-annealed film (black solid line) and photobleached film (grey dotted line).

EFFECT OF DEFECTS ON FILM EMISSION

Emission spectra were taken for di-alkyl polyfluorene thin films that underwent identical treatments as the thicker films used for the FTIR studies; all three overlaid spectra of PFO are shown in Figure 2.2. The pristine PF films had the expected structured blue emission characteristic for all di-alkyl polyfluorenes, with maxima at 426 nm, 450 nm and 480 nm. Photobleaching of the films, which created the greatest number of defects shown by FTIR, resulted in a new broad peak with a maximum centered at 525 nm, coupled with a significant decrease in the structured blue peaks. The overall intensity of fluorescence dropped dramatically for the photobleached film as it was damaged, and it had to be plotted on a separate axis in Figure 2.2 to illustrate the changes in the overall shape of the film emission. Thermal annealing in air of the films to their liquid crystalline phase transition temperatures (170 ˚C for PFO, 250˚C for PFH) resulted in a less dramatic decrease of the blue emission with the appearance of the green peak, confirming that not as many defects were created thermally as through photobleaching. Emission spectra for PFH under the same treatment as PFO had identical results, and are not shown.

Films were also annealed under nitrogen in an attempt to prevent defect formation; these films showed a very slight increase in green emission, with no evidence for the ketone stretch in IR spectra. This is not an indication that defects weren't created, but rather that the number of defects created was beneath the detection limit of the FTIR, which could explain the previous results seen.[24-27] PF films were also annealed under vacuum to eliminate the creation of defects, fluorescence of these films did not produce an increase in green emission, only a slight red-shift in the overall fluorescence emission

as the polymer chains were in a more extended configuration, showing that the removal of oxygen inhibits defect formation.

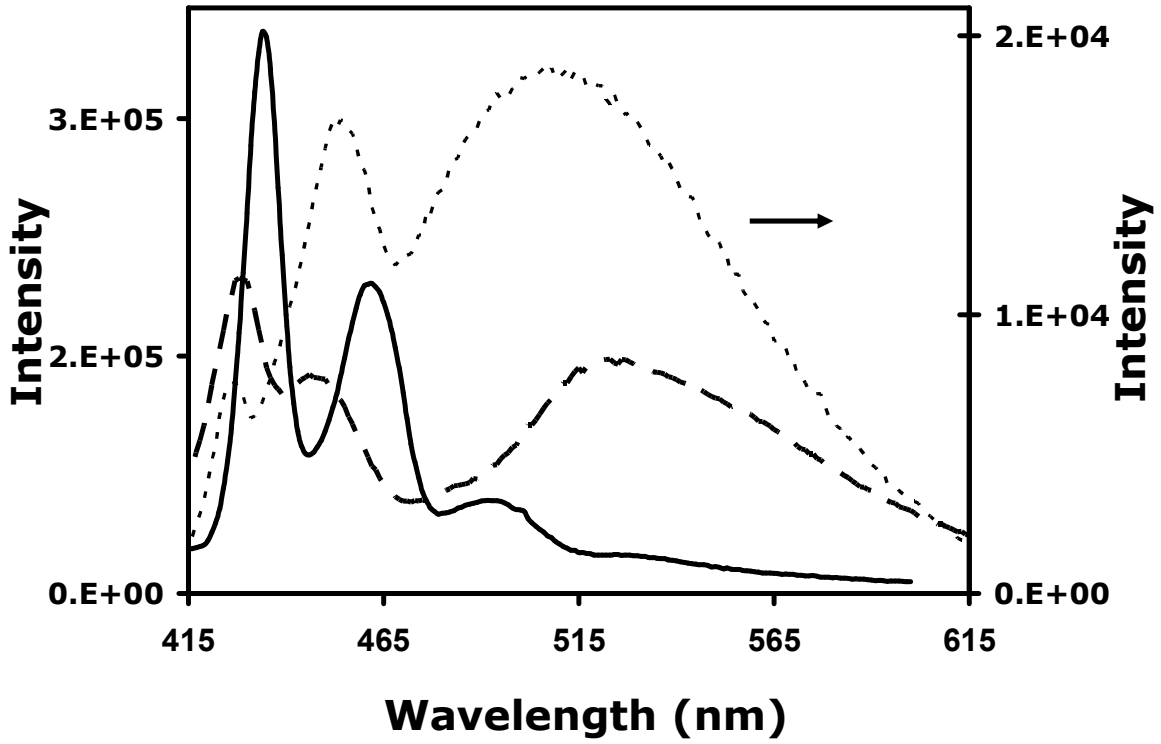

Figure 2.2 Emission spectra of polyfluorene pristine film (solid line), air-annealed film (long dashed line) and photobleached film (short dashed line). The growth of the green peak is evident in both air-annealed and photobleached films; the intensity of the photobleached film is plotted on a separate axis to show the relative structure of the peaks.

DILUTE POLYMER PHOTOBLEACHING EXPERIMENTS

Having confirmed that oxygen-based defects were the source of green emission in the PF films, the relation between polymer chain interactions and green emission was then investigated. Sims et al. had shown evidence for the excimer-based defects by

photobleaching of dilute PFO films,[17] where the polymer chains were isolated from one another in an inert polystyrene matrix. Similar experiments were performed on dilute PFO and PFH in a polystyrene or PMMA matrix using various solvents, with the polymers mixed at 0.06% (w/w) in relation to the matrix polymer, with the matrix polymer used as a 4% (w/w) solution in either toluene or tetrahydrofuran (THF). Dilute solutions of PFH and PFO behaved in a similar manner upon photobleaching (Figure 2.3, A and B respectively); a decrease in blue emission was seen with a small increase in the green area of the spectrum; while not a well defined peak as seen in the bulk film, this increase is apparent when the two spectra are normalized to the initial blue vibrational peak, shown in the Inset for each graph of Figure 2.3. The increased green emission coupled with a significant decrease in the blue emission revealed that efficient intramolecular energy transfer occurred from pristine chromophores to defect sites after the defects were formed through photobleaching. This supports evidence seen in the single molecule and oligomers studies.[18-24] In order to see if "intermolecular" energy transfer will occur with a single polymer chain interacting with itself, in a coiled or globular conformation, in addition to the intramolecular energy transfer for chains in an extended conformation, further studies were performed by comparing photobleached emission spectra for dilute films prepared in different solvents.

Fluorescence anisotropy data was collected for dilute films of 0.1% of polyfluorene in the PS matrix, using either toluene or THF as the solvent in order to determine the chain conformation in the different solvents. Films in toluene had a calculated anisotropy value of roughly 0.4, while this is a low value indicating a large amount of disorder was in the film, the 0.4 value indicates that the polymer chains were in an extended, linear configuration and emitted polarized light.

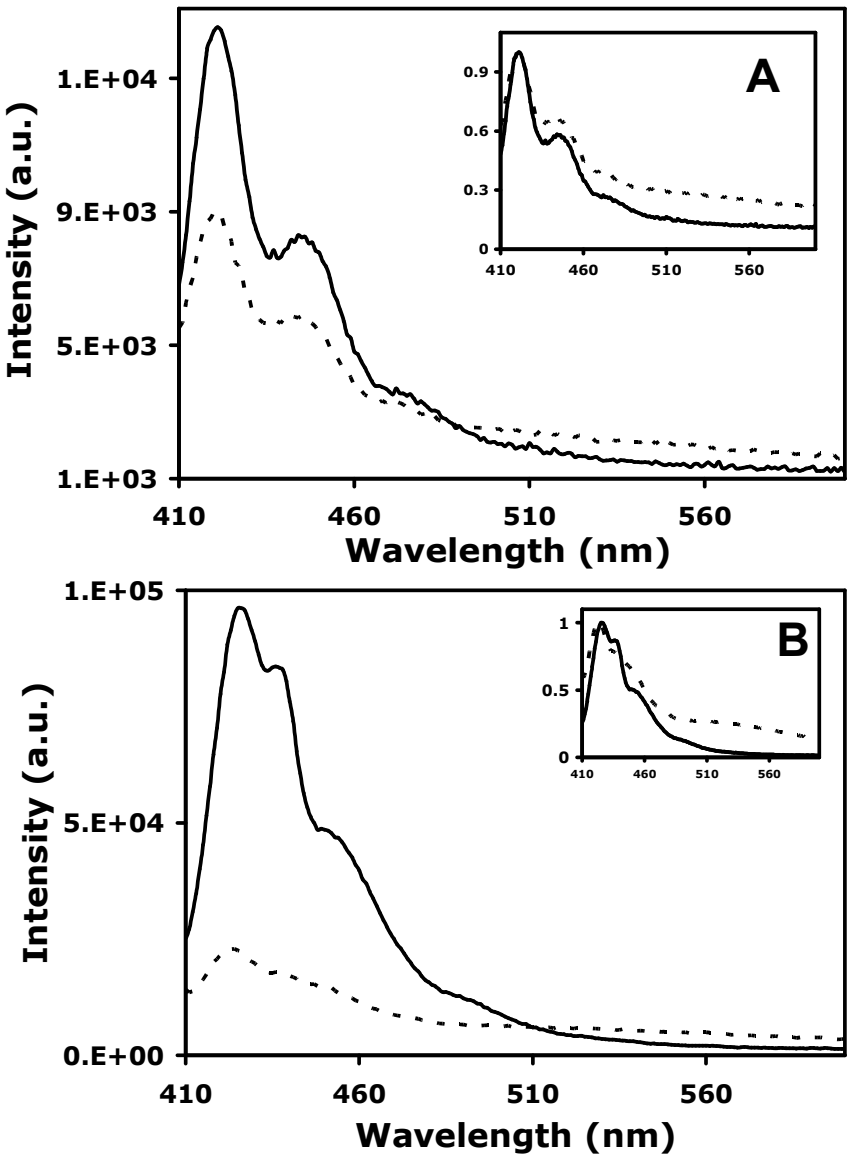

Figure 2.3 Dilute (0.6% in PS) PFH (graph A) and PFO (graph B) emission spectra prior to photobleaching (solid line) and after photobleaching for 80 minutes under a UV lamp (dashed line), showing a slight increase in the green portion of the spectrum for both polymers. Inset: Before and after spectra normalized to the first blue peak to illustrate the increase in the green for both polymers.

The calculated anisotropy value for polyfluorene in THF solvent, considered a poor solvent for PFs, was 0.06, showing that the individual chains were in a globular formation, which created contact points between parts of the chain in different orientations relative to one another. The globular configuration of PFs in THF led to energy transfer between differently orientated parts of the chain, creating light emitted in random orientations, providing little polarized emission. Bleaching of the dilute PF films with the polymer chains in a globular conformation led to a decrease in blue emission with no apparent increase in green emission, indicating no energy transfer from pristine chromophores to created defects, but these films were much more resistant to photobleaching compared to the dilute films in toluene, which did show an increase in green after photobleaching. Possible explanations for the discrepancies between the two films include: the defects formed on globular chains weren't emissive, or that the globular nature of the polymer chains inhibited the formation of many ketone defects.

IN-SITU ANNEALING OF POLYFLUORENE FILMS, EFFECT OF FILM ORDER ON EMISSION

The globular conformation of dilute PF chains might not have the same degree of chromophore interaction as can occur between the multiple closely packed chains in an ordered film. Unfortunately there is a major setback for making direct comparisons between different emission spectra in order to see the effect of order on emission: the fact that both the blue and green peaks change simultaneously and to different degrees during these experiments. Simply examining the same film before and after annealing is insufficient, as the fluorometer used to measure emission is highly sensitive to minor changes in film thickness, topography, and angle of the incident beam relative to the film. Although these minor changes will not affect the ratio of the peaks to one another, the

overall intensity will be changed, making a direct comparison impossible when there are only minor changes occurring in the emission spectra. The morphology studies were focused on PFH, as it showed the highest degree of order upon annealing, and thus would show the greatest effect of order in relation to defects.

In order to directly compare emission spectra before and after annealing of polyfluorene films, thermal annealing of polyfluorene films was done in the fluorometer using a homebuilt heating cell designed to be purged with an inert gas. Fluorescence spectra were collected in situ throughout the annealing process. Films previously annealed under nitrogen were not entirely free of water contamination, resulting in film defects; thus in situ experiments were performed under dried nitrogen or dried argon gas. For the most accurate comparison of emission intensities before and after annealing, corrections must be made for any changes in the film's absorbance at the excitation wavelength. Absorbance spectra taken for the thin films before and after annealing under the dried gas showed a slight decrease in absorbance after annealing, likely due to the ordering of the polymer chains that have polarized the absorption. Since the ordered domains are larger than the wavelength of light, and highly polarized, the minimum transmission for these regions will be 0.5, and corrections must be made to the absorbances. The absorbance spectra for PFH, taken before and after annealing, are shown in Figure 2.4, with graph A corresponding to the film annealed under dried argon.

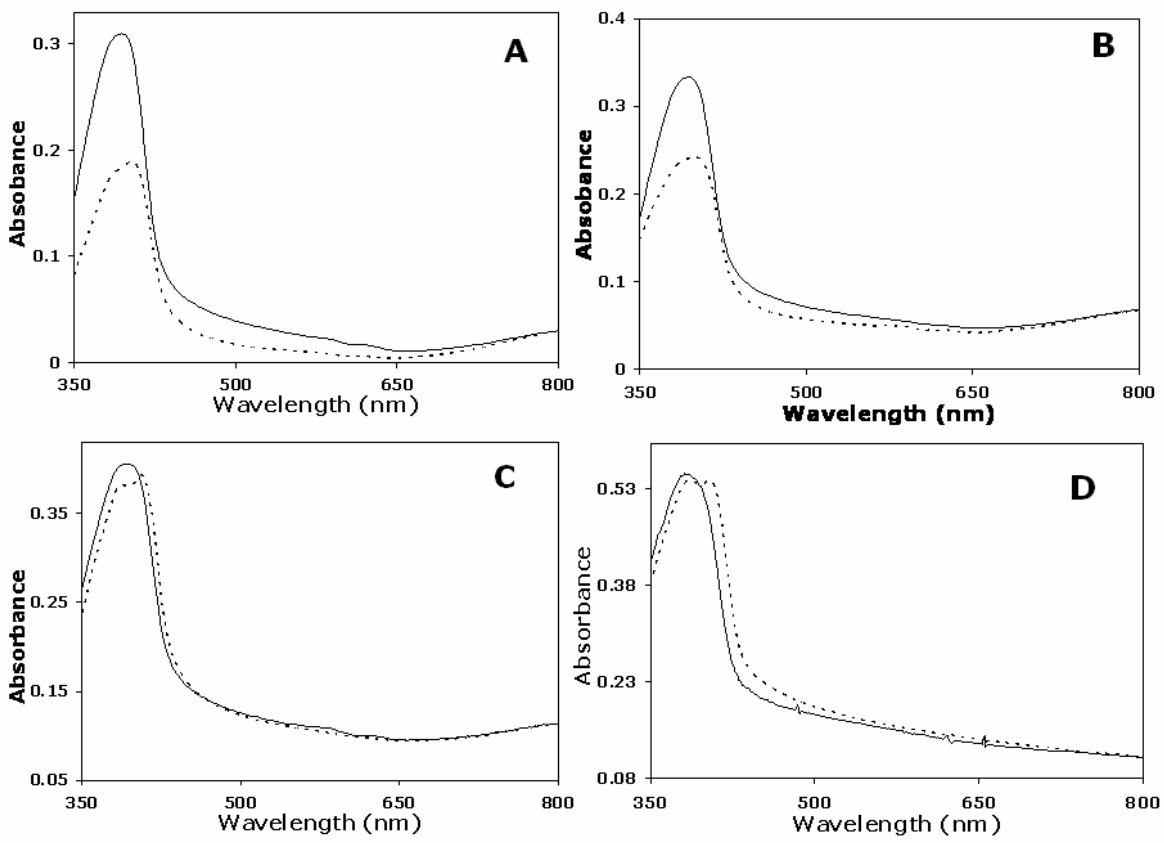

Figure 2.4 Absorbance spectra for PFH films prior (solid line) and after annealing (dashed line), for pristine films annealed under dried argon at 250˚C (A), in air at 250˚C (B), and for partially bleached films annealed under dried argon at 250˚C (C) and at 150˚C (D). With the exception of (D), all films have an apparent decrease in absorbance after annealing.

Emission spectra taken in situ for the film annealed under dried argon are shown in Figure 2.5, with the annealed emission corrected for its decreased absorbance. The corrected, annealed emission had a higher intensity compared to that of the pristine film, indicating a slight increase in quantum yield ( ). This has been seen previously,[28] and is believed to be from an extended conjugation length of the polymer chains after annealing. Examination of the final, increased annealed fluorescence shown in Figure 2.5 makes it appear as though there has been an increase in green emission, however, when the two

spectra are normalized to the initial blue peak (Inset of Figure 2.5) they are indistinguishable, indicating that no defects were created after annealing for a prolonged period under inert atmosphere.

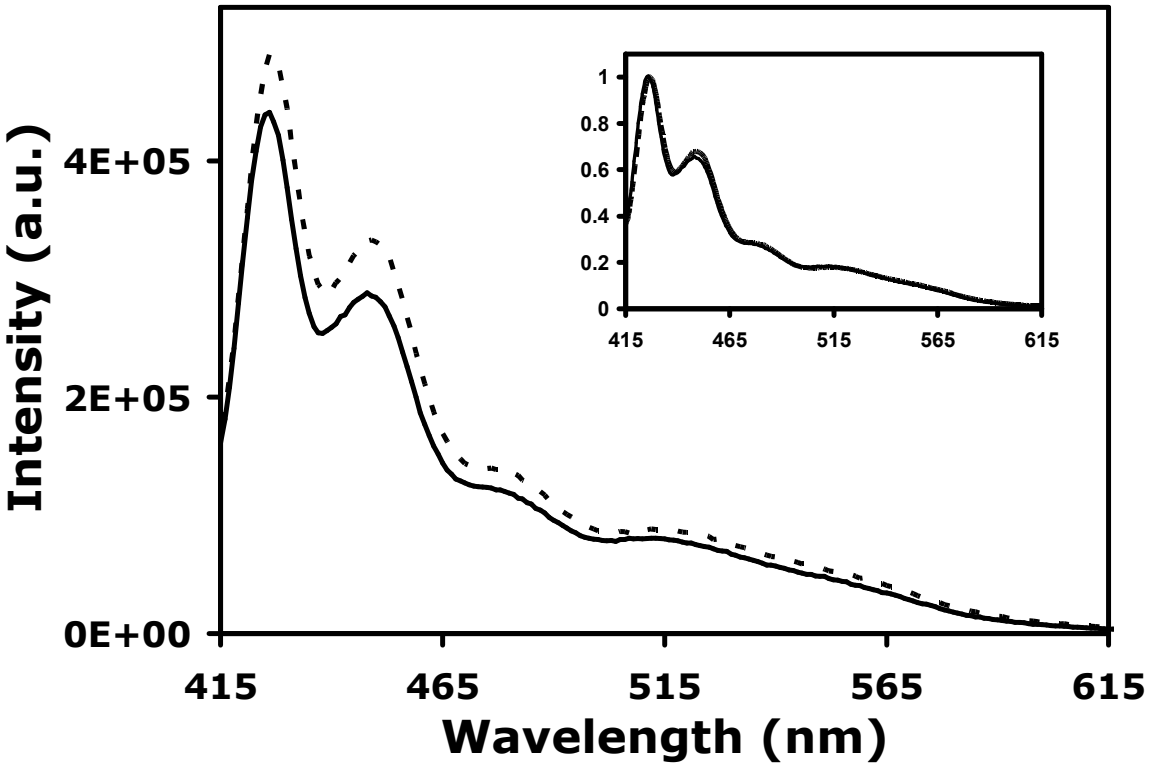

Figure 2.5 In situ, corrected fluorescence spectra for a PFH film, taken before (solid line) and after (dashed line) annealing, showing a slightly increased quantum yield. Inset: The spectra normalized to the first vibrational peak, showing identical overlay and no creation of ketone defects.

In situ spectra were also taken for films annealed in air to see the quantitative changes of emission spectra from defect formation. Air annealed films had a significant decrease in overall emission, coupled with the growth of a small peak at 525 nm, the corrected spectra are shown in Figure 2.6; the absorbance decrease was similar to that of

films annealed in dried argon. Since the in situ data reveals the absolute changes in emission, it can be seen that the few defects formed thermally are highly effective at quenching the blue emission while not being highly emissive themselves. The normalization of the two spectra to the first vibrational peak are shown in the inset of Figure 2.6, placing an emphasis on the green peak and making it appear as though the green emission is dominating the overall color of fluorescence, rather than the fluorescence decreasing overall, as can be seen in the absolute fluorescence shown for the in situ data.

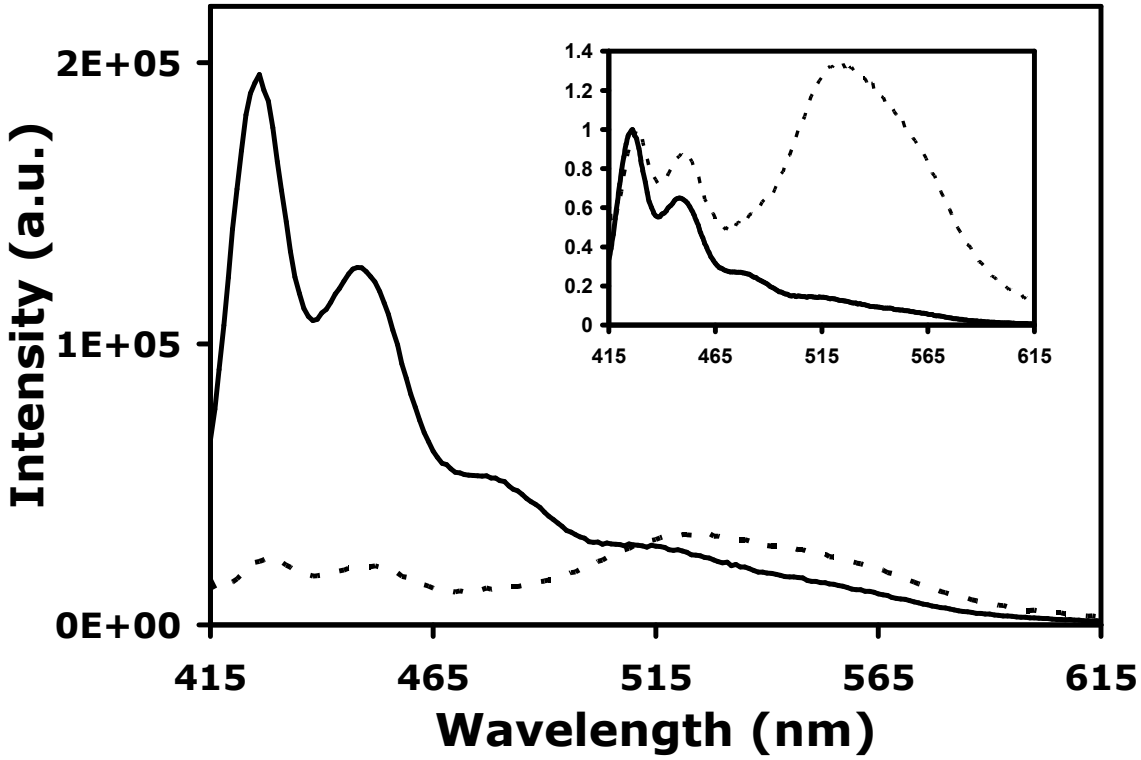

Figure 2.6 In situ, corrected emission spectra of a PFH film prior (solid line) and after (dashed line) annealing in air, showing the overall decrease in intensity. Inset: when the two spectra are normalized, it appears as if the green emission is abundant.

Since there is no evidence of defects created when films are annealed under dried argon, it was possible to examine how increased polymer order within a film containing some defects affected the overall emission. If the green emission was dependent only on the formation of defects and intrachain energy transfer, then ordering of a film containing some defects would not change the relative amounts of blue and green emission, however, if intermolecular energy transfer occurs after ordering, changes in the in situ data will be apparent. A small number of defects were created by photobleaching a thin PFH film beneath a UV lamp for forty minutes; sufficient to produce a new, broadened green peak around 520 nm while not significantly quenching the blue structured peaks. Adjusting the emission spectra for the minimal difference in absorbances did not change the final emission, shown in Figure 2.7. Prior to annealing, the small green peak is not particularly noticeable; after annealing the intensity of the blue emission decreased by half, with a simultaneous, relatively smaller increase seen in the green emission. Since the absolute changes in intensity can be compared for the in situ data, it is apparent that the intensity of the green emission has increased, but the most significant change has been the large relative decrease in the blue emission.

No defects were created in this film during the annealing process in the inert atmosphere, so the changes in emission spectra could only be caused by the ordering of the polymer chains upon annealing of the film to its liquid crystalline temperature. This increase in the green emission also is not due to an increase in quantum yield, as that would have led to an increase in the blue emission as well. The only explanation for the decrease in blue emission coupled with an increase in green emission is that the blue excited state is more efficiently transferred to the lower energy defect sites from the chains packing closely together after annealing. It has been shown that polymer chain order affects charge transport within films, with research and theoretical models

indicating that increased order increases the "hopping" of excitons between chains.[29-33] It has also been shown that ketone sites behave as low energy traps, where intrachain energy transfer was efficiently funneled from pristine chromophores to ketones on a single chain.[21]

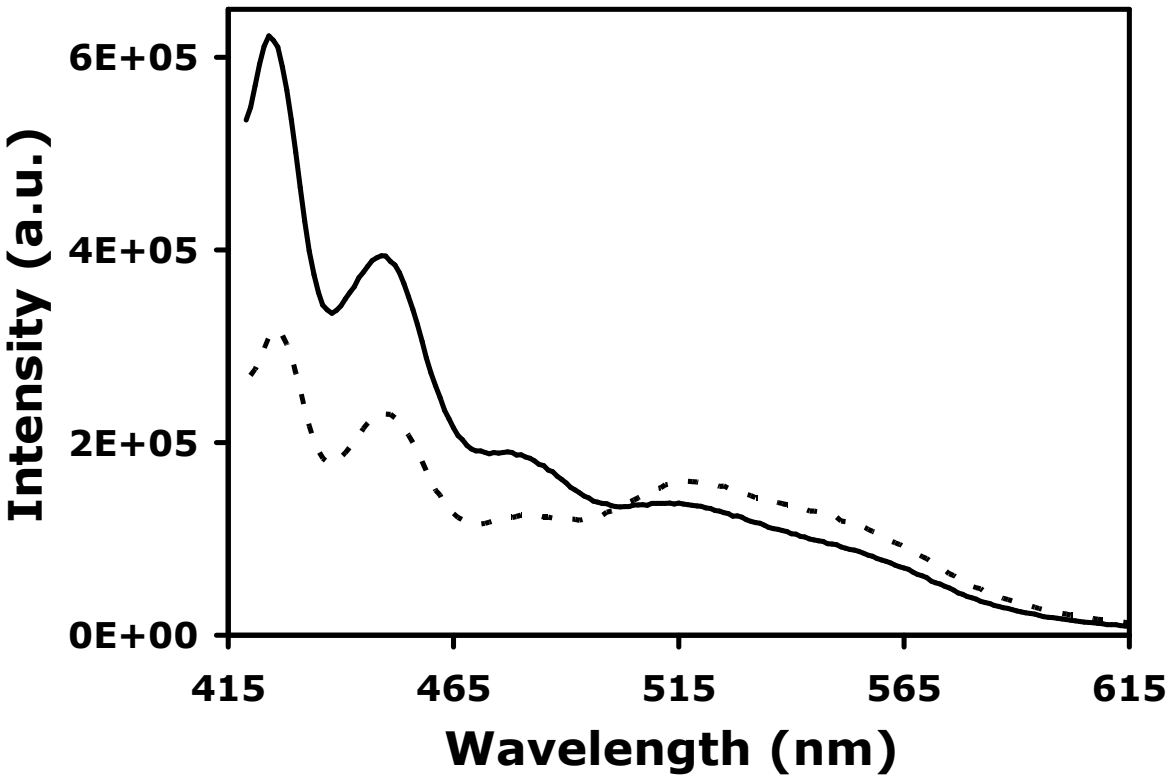

Figure 2.7 Corrected in-situ data for a partially bleached PFH film before (solid line) and after (dashed line) annealing under dried argon at 250˚ C for two hours. The blue emission has decreased with a corresponding small increase in green emission, evidence that ordering the film increased the quenching ability of the ketone defects.

ORDER WITHIN ANNEALED PF FILMS

The degree of order for the pristine and annealed films was measured through polarization anisotropy measurements for further confirmation that the varied film treatments are still ordering the film after annealing; as these films were examined for birefringence, anisotropy provides slightly more information on the degree of order within the bulk of the films for comparison. Pristine PF films have a calculated anisotropy value of ~0.04, shown below in Figure 2.8, along with the anisotropy measurements for all of the films. This low anisotropy is indicative of the amorphous nature of the film, where energy is transferred quickly among the disordered polymer segments and emitted in random orientations, nearly washing out any polarization. The annealed films show increased order, with anisotropy values of 0.14 for films annealed under the dried argon or in air. The anisotropy is fairly constant over the green peak in the air annealed film, but the anisotropy for the green peak of the partially bleached annealed film is also constant and higher, at 0.2, with the largest anisotropy seen for any of the films. The fact that the large anisotropy remains constant over the green emission implies that it is polarized in the same direction as the absorbance, and it indicates that the energy transfer is occurring predominately within the ordered domains where the polymer chains have identical orientation. This is evidence for the increased energy transfer from pristine chains to defect sites upon annealing of the partially bleached film. It is also of note that the films annealed under dried argon contain a large peak along the blue edge of the spectrum; this is the result of emission from the highest energy chromophores, which cannot be populated by energy transfer, but instead are directly excited and emit immediately showing a higher degree of polarization.

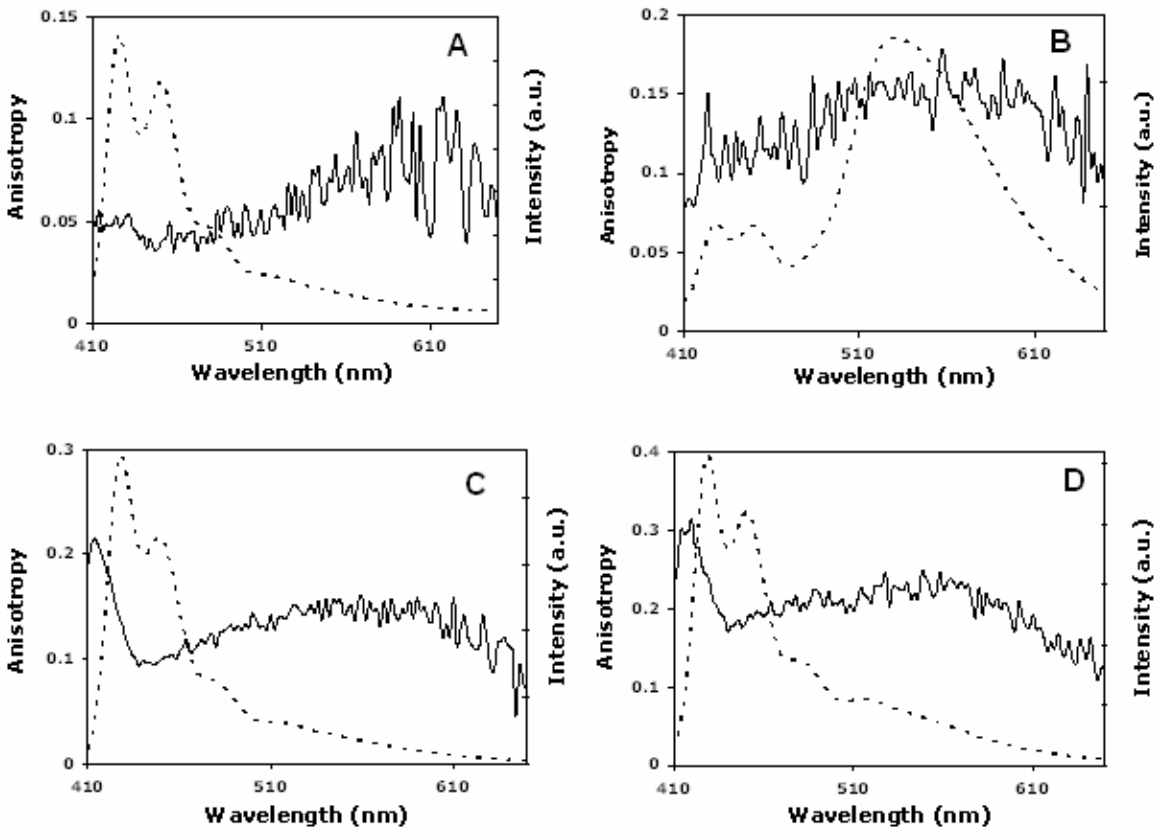

Figure 2.8 Anisotropy (solid line) plotted against film emission (dashed line) for a pristine film (A), air annealed film (B), annealed in dried argon (C) or partially bleached film annealed under dried argon (D). Larger values are seen for the annealed films.

EMISSION CHANGES AND ORDERED FILMS

To show that the changed morphology was the source of the spectral changes in the partially bleached films, an identical partially bleached film was annealed below the liquid crystalline (LC) phase transition temperature of 250˚C for PFH. At this temperature, the film would undergo heating with minimal reordering of the polymer chains. The partially bleached PFH film was annealed under dried argon at 150˚C for

two hours, similar to the films annealed at the LC temperature. In situ data for the lower temperature annealed film is shown in Figure 2.9, along with AFM topography scans. The adjusted emission spectra showed a small increase in quantum yield upon heating, similar to the pristine PFH film annealed under dried argon. Unlike the film annealed to the LC temperature, there was no change in the relative intensities of blue and green emission, indicating that the film did not order sufficiently for increased energy transfer to defects. This is confirmed in the inset of Figure 2.9, where the final annealed emission is normalized to the initial emission to have an identical overlay between the two. Furthermore, the low temperature annealed film did not exhibit any birefringence between crossed polarizers, unlike the ordered LC temperature annealed film. As seen in the AFM scans of Figure 2.9, the topography of the low temperature annealed film is very similar to that of a pristine film, rough and disordered. This is in stark contrast to the film annealed at 250˚C, where the polymer chains have ordered into aligned, ribbon-like structures. The previous work using NSOM have demonstrated that these ribbon-like structures are composed of aligned polymer chains.[6] Thus it is apparent that the increased green emission and decreased blue emission for the partially bleached films annealed at the LC temperature resulted from the increased polymer order. Without the tightly-packed domains formed at the LC temperature, the only change is a slight increase in quantum yield, explained by an extended conjugation length of the polymer chains.[28]

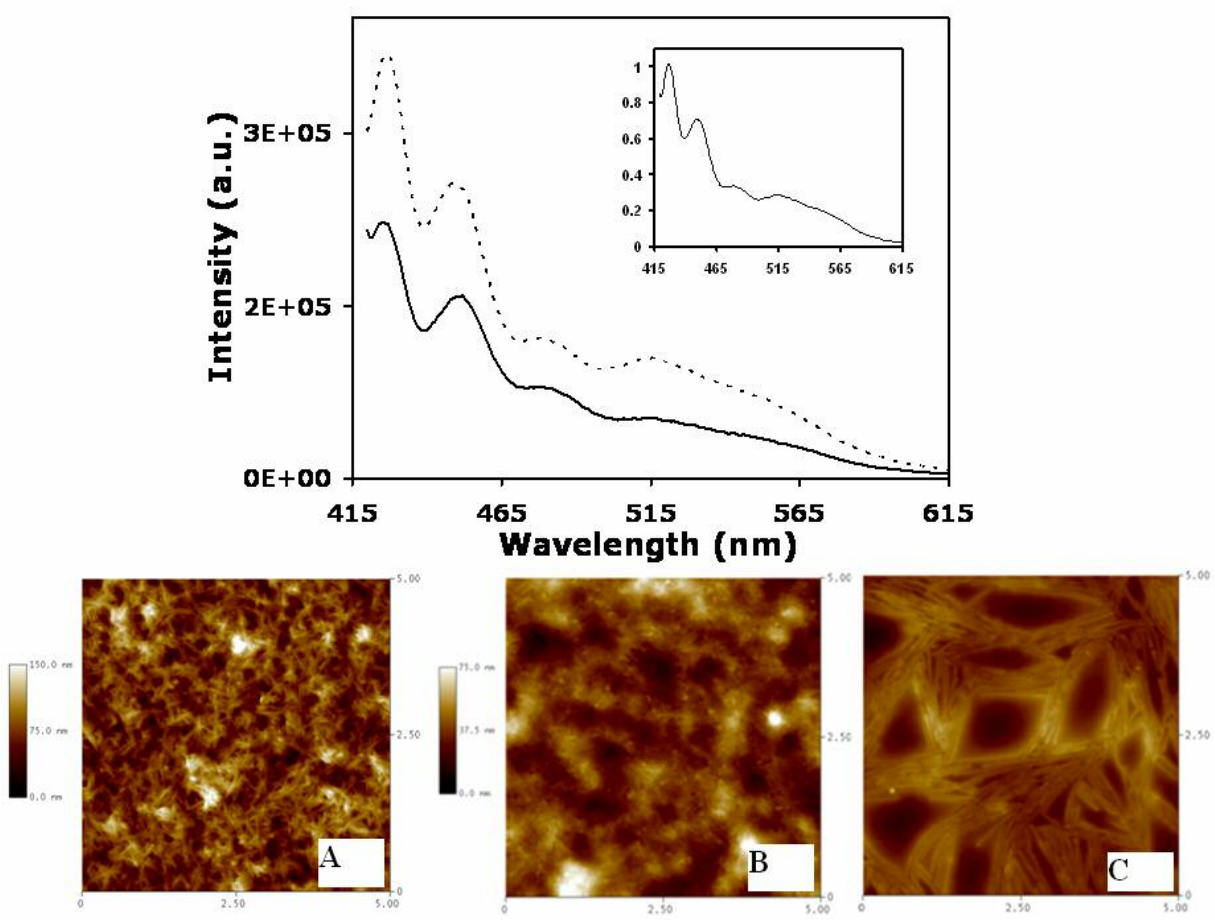

Figure 2.9 Corrected in situ spectra for a partially bleached PFH film annealed at 150˚C for two hours before (solid line) and after (dashed line) annealing. Inset: Normalization of the two spectra shows no change in the relative blue to green ratios. AFM scans of pristine PFH film (A), film annealed at 150˚C (B) and film annealed at 250˚C (C), showing the rough disordered topography for A and B, and the ordered, ribbon-like domains in C.

CONCLUSIONS

Di-alkyl polyfluorene films showed evidence of chemical defects formed through photobleaching or thermal annealing of films in air, with evidence that only a few defects

could have a substantial effect on film emission. Photobleaching experiments of dilute polymer films gave evidence that single polymer chains could produce some green emission, indicating effective energy transfer from pristine chromophores to defects on individual chains. PFH films, showing a higher degree of order for di-alkyl polyfluorenes with various lengths of sidechains, were then examined for the effect of increased film order on chemical defects. These films were annealed to their LC temperature in situ, allowing for a direct comparison between absolute changes in their emission spectra. There was no evidence of ketone defect formation for films annealed under dried argon, thus it was possible to monitor the effect of increased polymer chain order on emission of a film already containing a small number of defects. Subsequent ordering of the film containing defects led to an increase in green emission and decrease in blue emission, indicating that the increased order resulted in a greater amount of energy transfer from pristine chains to defect sites. Exciton energy migration within the polyfluorene films was shown to increase within the aligned polymer domains, allowing for a more efficient funneling of the energy to the ketone traps. The increased energy transfer between the closely aligned chains, while important to how PLEDs function, has relevance to other polymer systems. An example would be mixed polymer solar cell films, where it is extremely important to maximize the amount of exciton diffusion in different polymer domains to produce a more efficient device.

EXPERIMENTAL

Sample preparation

Poly(9,9-dihexylfluorene) from the Dow Chemical Company was used without further preparation. Solutions were made by dissolving the polymer in solvent, then

heating briefly to clarity to ensure full dissolution. Thick films used for FTIR measurements were dropcast onto aluminum or gold coated silicon wafer from 1% (w/w) solutions of PF in chloroform to produce ~1μm thick films. Thin films did not produce strong enough IR stretches to be measured over the background, necessitating the thicker films. Thin films used for all fluorescence measurements were spincast from the 1% (w/w) solution onto base-cleaned glass coverslips or quartz substrates at 2000 rpm for 40 seconds. All photobleached films were placed in close proximity to a UV lamp (~2 cm), and bleached for 40 minutes (partially bleached films) or for 2 hours (bleached films). Annealed films were kept within ±1˚C of the LC temperature (or lower temperature) for two hours; if annealed under gas, then the films were purged one hour prior to annealing, and were purged during the cooling process to room temperature.

Instrumental

FTIR spectra were taken on a Thermo Mattson Infinity Gold FTIR, using a Pike Technologies Veemax II variable angle grazing accessory at 60˚ incident angle. The grazing angle accessory allows for more of the film to absorb the IR light, as the beam is directed through a series of mirrors to enter the film at an angle relative to the substrate, which then passes through a large amount of the film and is reflected off of the gold or silver coating to be directed into the detector. The angle at 60˚ was found to give the strongest IR signal and was used for all of the films measured.

In situ fluorescence measurements were taken using a SPEX DM3000 Fluorometer in front-face mode, with a homemade holder that could be purged with gas and a thermocouple-regulated heat source. Thin films on quartz substrates were sealed within the holder so that the film could be purged with dried argon, with the excitation light passing through the quartz substrate to excite the polymer film, minimizing surface

roughness effects. The holder was affixed in place within the fluorometer and remained untouched during the measurements. Absorbance spectra of the films were collected on a Cary 5000 UV-VIS NIR spectrometer before and after annealing, and underwent baseline correction. Topography measurements were taken on a Digital Instruments Multimode AFM in tapping mode.

Anisotropy measurements were taken in the fluorometer, by measuring fluorescence of the film through polarizers, collecting data for the equation shown below. The films are placed between two polarizers, either with the two polarizers vertically parallel (Ivv), or crossed (Ivh). The G factor is calculated as the difference in emission intensities for horizontally polarized emission (Ihv/Ihh), to correct for the fact that the detector absorbs emission that is polarized in the horizontal plane more efficiently, accounting for the horizontally polarized light in the x and z directions. Both the G factor and the vertical intensities are measured over the entire film emission and plotted against the film emission to give the average anisotropy for the film.

$$\text{Anisotropy} = \frac{Ivv - G(Ivh)}{Ivv + 2G(Ivh)}$$

Equation 2.1 Anisotropy calculation for bulk film measurements.

REFERENCES

1. V. N. Bliznyuk, S. A. Carter, J. C. Scott, G. Klärner, R. D. Miller, and D. C. Miller, *Macromolecules* **1999**, *32*, 361.

2. K. H. Weinfurtner, H. Fujikawa, S. Tokito, and Y. Taga, *Appl. Phys. Lett.* **2000**, *76*, 2502.

3. J. I. Lee, G. Klärner, and R. D. Miller, *Synth. Met.* **1999**, *101,* 126.

4. Q. B. Pei, and Y. Yang, *J. Am. Chem. Soc.* **1996**, *118*, 7416.

5. U. Lemmer, S. Heun, R. F. Mahrt, U. Scherf, M. Hopmeier, U. Siegner, E. O. Göbel, K. Müllen, and H. Bässler, *Chem. Phys. Lett.* **1995**, 373.

6. J. Teetsov and D. A. Vanden Bout, *Langmuir* **2002**, *18*, 897.

7. M. Grell, D. D. C. Bradley, G. Ungar, J. Hill and K. S. Whitehead, *Macromolecules* **1999**, *32*, 5810.

8. V. Cimrová, U. Scherf, and D. Neher, *Appl. Phys. Lett.* **1996**, *69*, 608.

9. E. J. W. List, R. Güntner, P. S. de Freitas, and U. Scherf, *Adv. Mater.* **2002**, *14*, 374.

10. X. Gong, P. K. Iyer, D. Moses, G. C. Bazan, A. J. Heeger, and S. S. Xiao, *Adv. Funct. Mater.* **2003**, *13*, 325.

11. S. I. Hintschich, C. Rothe, S. Sinha, A. P. Monkman, P. S. de Freitas, and U. Scherf, *J. Chem. Phys.* **2003**, *119*, 12017.

12. J. M. Lupton, M. R. Craig, and E. W. Meijer, *Appl. Phys. Lett.* **2002**, *80*, 4489.

13. E. Zojer, A. Pogantsch, E. Hennebicq, D. Beljonne, J. L. Bredas, P. S. de Freitas, U. Scherf and E. J. W. List, *J. Chem. Phys.* **2002**, *117*, 6794.

14. X. Gong, D. Moses, A. J. Heeger and S. Xiao, *Synth. Met.* **2004**, *141*, 17.

15. F. B. Dias, M. Maiti, S. I. Hintschich and A. P. Monkman, *J. Chem. Phys.* **2005**, *122*, 054904.

16. L. Romaner, A. Pogantsch, P. S. de Freitas, U. Scherf, M. Gaal, E. Zojer and E. J. W. List, *Adv. Funct. Mater.* **2003**, *13*, 597.

17. M. Sims, D. D. C. Bradley, M. Ariu, M. Köberg, A. Asimakis, M. Grell and D. G. Lidzey, *Adv. Funct. Mater.* **2004**, *14*, 765.

18. A. Pogantsch, N. Zaami and C. Slugovc, *Chem. Phys.* **2006**, *322*, 399.

19. K. Becker, J. M. Lupton, J. Feldmann, B. S. Nehls, F. Galbrecht, D. Gao and U. Scherf, *Adv. Funct. Mater.* **2006**, *16*, 364.

20. C. Chi, C. Im, V. Enkelmann, A. Ziegler, G. Lieser and G. Wegner, *Chem. Eur. J.* **2005**, *11*, 6833.

21. F. B. Dias, M. Knaapila, A. P. Monkman and H. D. Burrows, *Macromolecules* **2006**, *39*, 1598.

22. E. Aharon, A. Albo, M. Kalina and G. L. Frey, *Adv. Funct. Mater.* **2006**, *16*, 980.

23. F. Montilla and R. Mallavia, *Adv. Funct. Mater.* **2007**, *17*, 71.

24. J. Teetsov and D. A. Vanden Bout, *Langmuir* **2002**, *18*, 897.

25. J. Teetsov and D. A. Vanden Bout, *J. Am. Chem. Soc.* **2001**, *123*, 3605.

26. J. Teetsov and M. A. Fox, *J. Mater. Chem* **1999**, *9*, 2117.

27. J. Teetsov and D. A. Vanden Bout, *J. Phys. Chem. B.* **2000**, *104,* 9387.

28. K. Asada, T. Kobayashi and H. Naito, *Jpn. J. Appl. Phys.* **2006**, *45*, L247.

29. E. Hennebicq, G. Pourtois, G. D. Scholes, L. M. Herz, D. M. Russel, C. Silva, S. Setayesh, A. C. Grimsdale, K. Müllen, J. L. Bredas and D. Beljonne, *J. Am. Chem. Soc.* **2005**, *127*, 4744.

30. P. Sreearunothiaj, A. C. Morteani, I. Avilov, J. Cornil, D. Beljonne, R. H. Friend, R. T. Phillips, C. Silva and L. M. Herz, *Phys. Rev. Lett.* **2006**, *96*, 117403.

31. T-Q. Nguyen, R. Y. Yee and B. J. Schwartz, *J. Photochem. Photobiol. A.* **2001**, *144*, 21.

32. T-Q. Nguyen and B. J. Schwartz, *J. Chem. Phys.* **2002**, *116*, 8198.

33. B. J. Schwartz, *Annu. Rev. Phys, Chem.* **2003**, *54*, 141.

CHAPTER 3: FILM MORPHOLOGY IN DI-ALKYL POLYPHENYLENE ETHYNYLENE LIGHT EMITTING DEVICES (LEDS)

BACKGROUND

Conjugated polymers based on phenylene ethynylene polymers and copolymers have shown considerable interest for use in optoelectronic devices, due to their chemical stability and high quantum yields.[1-6] Similar to other conjugated polymers often used in LEDs, polyphenylene ethynylene (PPE) polymers are liquid crystalline, forming into ordered domains upon thermal annealing of films.[7,8] Most rigid rod, liquid crystalline polymers often have complex interchain interactions upon annealing, affecting their semiconducting properties such as charge transport within the film and shifting the fluorescence emission.[9-13] Straight sidechain di-alkyl polyphenylene ethynylenes such as poly[*p*-(2,5-didodecylphenylene)ethynylene] (DPPE)[7], and poly[*p*-(2,5-dinonylphenylene)ethynylene] (NPPE), initially have a broad, featureless green emission as pristine films. This type of emission is characteristic of aggregates or excimers, which are defined respectively as ground-state electronic interactions and excited-state electronic interactions between multiple chromophores. The broad green emission seen in DPPE films was initially debated and believed to be from aggregates,[14-15] but previous work on DPPE has shown a lack of ground-state interactions, concluding that the green emission was excimer-based emission.[7]

The most curious aspect of the di-alkyl PPEs is that the broad featureless green emission seen in the pristine film blue-shifts and becomes more structured after thermal annealing to resemble the single-chain emission seen in dilute solution, despite the fact that the films exhibit a high degree of order after annealing.[7] DPPE films were shown to

have the polymer chains pack closely together upon annealing to their liquid crystalline state, evidenced by film birefringence, x-ray crystallography data, and NSOM polarization data, so increased polymer chain interactions were expected based on the degree of order within the films, which would not have changed the green emission. A possible explanation for the combination of a high degree of order without evidence of interchain interactions could be through a unique packing order of the polymer chains; where the chains are staggered in a brick wall stacking motif, causing the chromophore backbones to be isolated from one another due to sidechain overlap of neighboring polymer chains, inhibiting electronic interactions between them, rather than through a more typical -stacking of the polymer chains which would have increased the excimer emission.[7] Fluorescence spectra from the shorter-sidechain NPPE behave in a manner similar to that of DPPE, and their emission spectra overlay the DPPE fluorescence spectra. Furthermore, NPPE also evidences a high degree of order upon annealing of the thin films.

Many researchers have examined PPE-based LEDs,[1-6,16-17] although few have mentioned any relation between morphology and electroluminescence.[17] Pristine LED electroluminescence for both PPE polymers matched their pristine photoluminescence, both dominated by the green excimer-based emission. The annealed DPPE LED EL is also dominated by this green emission, despite the fact that the photoluminescence shows no evidence for excimers. A difference is seen in the electroluminescence of the annealed NPPE LEDs, which produce a more structured, slightly blue shifted EL compared to their pristine EL, but which is still redshifted relative to the photoluminescence (PL) and containing a shoulder in the excimer region. Since the broad green emission has been identified as excimer-based, the green emission seen in the DPPE LEDs must be from the excimer species within the film. With far fewer

excimers seen in the well-ordered annealed films, and the electroluminescence dominated by these few excimers for the DPPE, the intensity of the electroluminescence and device function of the DPPE LEDs was decreased relative to the pristine devices. With the green excimer emission contributing a smaller portion to the annealed NPPE LED's EL, the annealed NPPE LEDs resulted in a higher EL intensity and increased function relative to the annealed DPPE LEDs. The differences between the shorter sidechain NPPE electroluminescence and the longer sidechain DPPE electroluminescence can only be explained through differences in the two polymer's morphology, considering that the photoluminescence spectra for the two polymers are identical, and the thin film LEDs were processed under the same conditions. It was seen that the shorter sidechain-containing polymers in polyfluorene studies contributed to an increased degree of order, it was then expected that the shorter sidechain NPPE would order to a greater degree relative to the DPPE. However, the DPPE films order to an excellent degree[7], and NSOM polarization anisotropy of NPPE films revealed a lower degree of order compared to the DPPE, so the differences in the EL spectra for the different polymer devices was not the result of their relative morphologies. The exact reason for their dissimilar electroluminescence spectra remains unknown.

PREVIOUS WORK ON DPPE

DPPE photoluminescence was examined thoroughly in solution and films, showing that it produced a bright blue photoluminescence in dilute solution, which then shifted to a broad, featureless green emission in pristine spincast films (for reference, an example of these spectral shifts is seen for NPPE in Figure 3.4). This red-shifted, broad green emission, characteristic of both aggregates and excimer species, was ultimately shown to be the result of excimers between close contacts of polymer chains in the film,

identified by an unchanged absorption spectrum after annealing and the long fluorescence lifetime of the emission. The blue-shifted emission was highly unusual, in that the DPPE films evidenced a high degree of order after annealing, seen by x-ray crystallography data, polarized NSOM fluorescence and film birefringence, and was explained through the brick-style packing motif, which is diagrammed in Figure 3.1. Only the vertical separation was determined by x-ray crystallography, at ~1.4 nm distance between the backbones,[7] so the lateral packing order of the chains was inferred from the spectroscopic data. As seen in Figure 3.1, most conjugated polymers pi-stack, producing increased electronic interactions between the polymer chains to produce aggregate or excimer emission. Since a decreased amount of electronic interaction was seen in the annealed DPPE films, it was theorized that the packing order was different from other conjugated polymers, where the backbones of polymer chains were isolated from one another by the sidechains of other polymer chains. This particular packing motif would produce the expected blueshifted, structured emission seen in the annealed DPPE films.

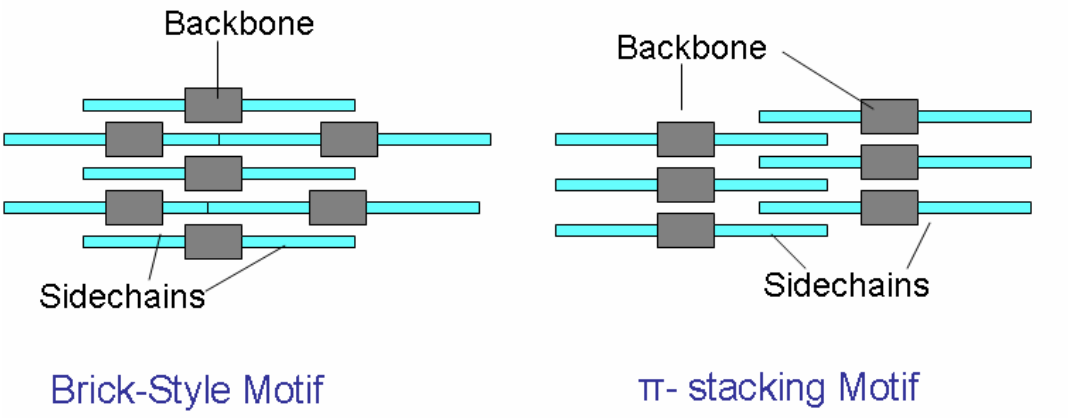

Figure 3.1 Comparison of the brick-style packing motif of annealed PPE polymer chains to the -stacking motif of other annealed LC conjugated polymers.

DPPE-BASED LIGHT EMITTING DEVICES (LEDS)

Considering that the electroluminescence produced by conjugated polymer films in devices is the result of the decay of singlet excitons (a spatially bound excited state formed from an electron- hole pair), which is not different in electronic structure from an excited state formed through light absorption, it is expected that electroluminescence spectra should be closely aligned with film photoluminescence. Research presented on similarly-structured MEHPPV devices[18-22] also expressed very similar EL to PL spectra, as have other popular but dissimilarly-structured polymers used in LEDs,[23-24] further support that EL spectra should be identical to PL spectra for the PPE devices.

Sandwich-type LEDs were produced using DPPE as the active layer. The sandwich devices were made with and without a thin layer of hole-transport material poly(3,4-ethylenedioxythiophene) poly(styrenesulfonate) [PEDOT-PSS] which was used in some films to enhance hole-injection. Aluminum was evaporated for the cathode; it had been shown by others that PPE polymers are more of an electron-transport material, due to the fact that alkoxy-PPEs made with various cathodes (Ca, Mg, and Al) performed best when used with only aluminum.[3] The di-alkyl based PPEs used in our studies also performed best when using aluminum solely as the cathode material. The electroluminescence spectra of a pristine and annealed DPPE device are shown in Figure 3.2. The pristine DPPE device EL spectrum is broad, green and featureless, identical to the pristine film photoluminescence, while the annealed DPPE EL overlaps the pristine EL, with a small amount of structured peaks seen along the blue edge of the spectrum.

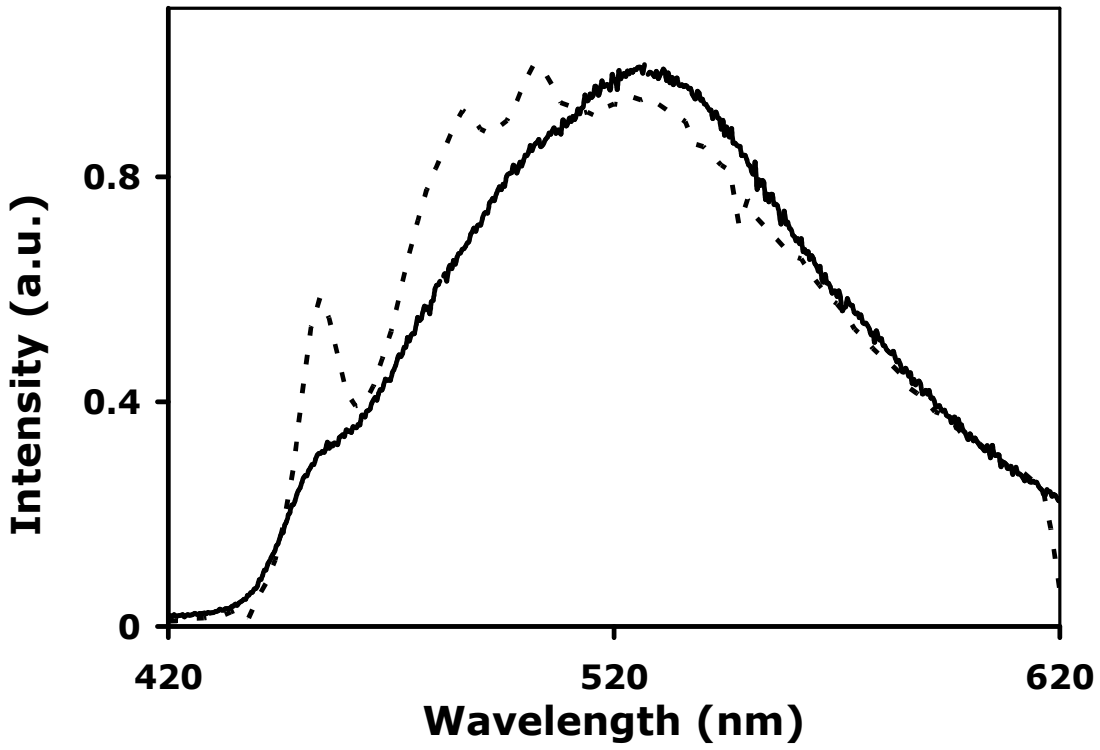

Figure 3.2 Green pristine DPPE electroluminescence (solid line) and green, slightly structured, annealed DPPE electroluminescence (dashed line). The peak maxima are very close, with the annealed peak's maximum slightly blueshifted.

The electroluminescence in both the pristine and annealed devices is dominated by the green excimer emission seen in the pristine DPPE photoluminescence, indicating that the excimer sites within the film behave as low energy traps, forcing the recombination of injected electrons and holes to occur preferentially at these sites. Annealing of the DPPE devices was performed in a glovebox, so the creation of possible defects in the film through heating was highly unlikely. Electroluminescence for some devices have exhibited efficient energy transfer to low energy trapping sites on polymer chains,[25-26] so it is reasonable to believe that is the case for the DPPE devices. The

maximum of the pristine DPPE EL is at 520 nm, and was compared to the photoluminescence spectrum taken from the same device, producing an identical overlay of the spectra. The annealed DPPE EL also has its maximum at ~ 520 nm, while the small structured peaks fall at maxima of 454 nm, 486 nm and 502 nm, slightly redshifted relative to their respective peaks seen from the photoluminescence taken for the same device, with those maxima occurring at 452 nm, 482 nm and 500 nm. The slight amount of structure seen in the annealed EL indicates that a small portion of the electroluminescence is produced from the higher-energy, electronically isolated chain emission sites seen in the photoluminescence.

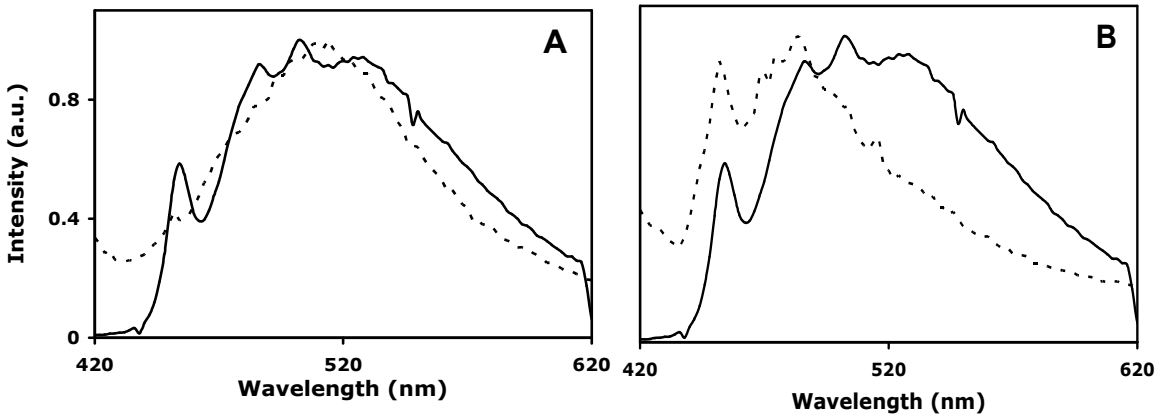

Figure 3.3 In graph A, the EL spectrum of a pristine DPPE LED (solid line) is overlaid with a pristine film's PL spectrum (dashed line), showing the similarity between the two. In graph B, the EL spectrum of an annealed DPPE LED (solid line) is overlaid with its own PL spectrum (dashed line), showing that the EL is different from its own PL, dominated by excimer emission.

Photoluminescence spectra were collected for the identical DPPE devices after electroluminescence spectra were collected in order to rule out any spectral differences in

films produced and annealed on ITO compared to the thin films produced on glass coverslips for previous fluorescence studies. The photoluminescence of a pristine DPPE LED overlaid with the electroluminescence of the annealed DPPE LED are shown in Figure 3.3, graph A, illustrating the similarity between the annealed EL to the pristine PL. The photoluminescence of the annealed device is blue-shifted with well-formed vibrational structure, matching the PL of films shown previously[7] for DPPE, and it is overlaid with the EL from the same device in Figure 3.3, graph B, illustrating the definite difference in shape and spectral shifts between the PL and EL of the same film. A comparison of the photoluminescence spectra of the device (shown as the dashed lines in Figure 3.3) reveals that their maxima are identical to those of PL spectra from thin DPPE films on glass, so it is apparent that the films prepared on ITO do not behave differently under annealing conditions compared to films made on glass substrates.

NPPE-BASED LEDS

NPPE photoluminescence spectra are similar to DPPE photoluminescence spectra; the three PL spectra, of NPPE in dilute solution, in a pristine film and in a annealed film are shown in Figure 3.4. The emission spectra of pristine and annealed NPPE films nearly overlay the maxima of the PL of DPPE films, showing the similarity in behavior for the two different polymers. Similar to the DPPE films, the NPPE PL have a structured blue emission in dilute solution, with maxima at 427 nm and 453 nm; a broad green, featureless emission in the pristine films with its maximum at 518 nm; and a blue-shifted, structured emission in the annealed films with peak maxima located at 455 nm, 482 nm, and 500 nm. These maxima either match those for DPPE emissions or are slightly blue shifted by a few nanometers. Also similar to DPPE, the NPPE films are birefringent when illuminated between crossed polarizers, showing that they also order

into domains upon annealing. Identical film treatments were performed on both NPPE and DPPE thin films and devices.

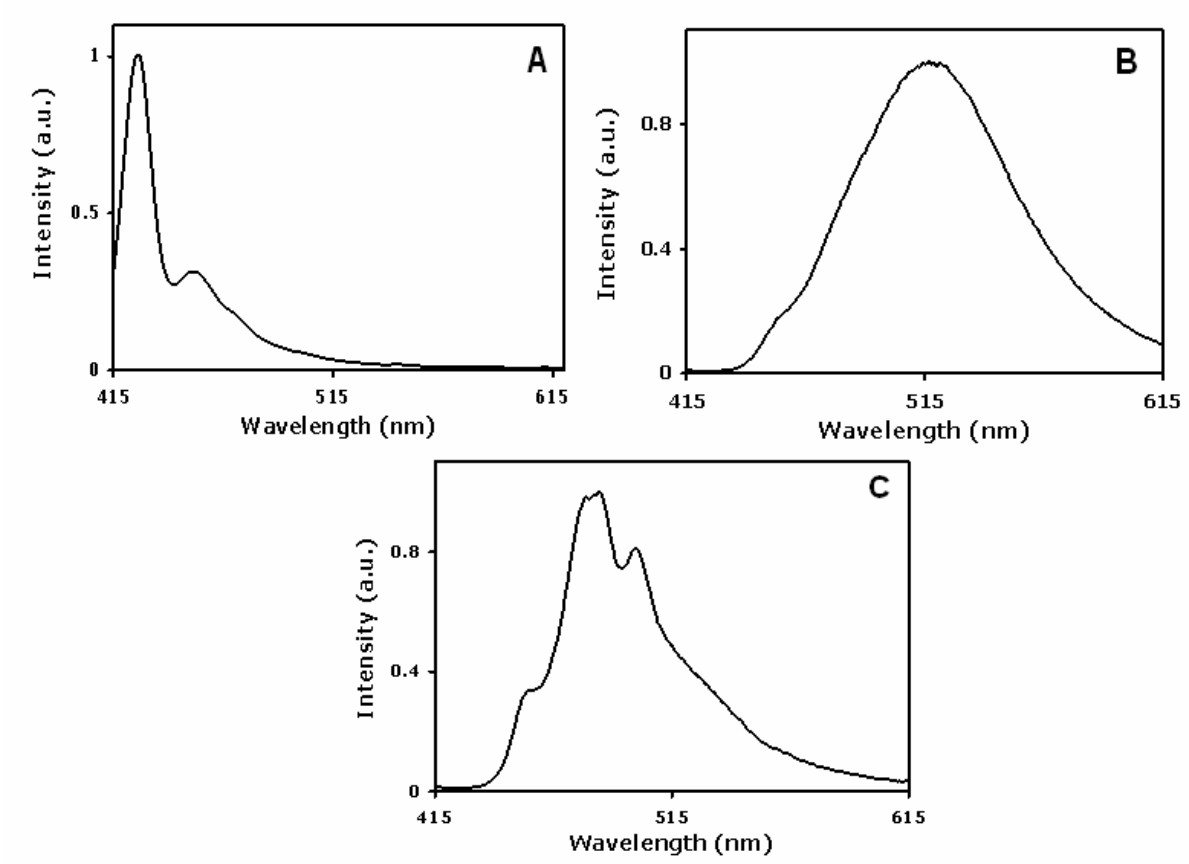

Figure 3.4 PL spectra of NPPE in (A) dilute solution, (B) pristine film and (C) annealed film, showing the various spectral shifts, similar to DPPE results reported previously.

The electroluminescence of a pristine NPPE device is broad, green and featureless, and unlike the DPPE EL, is slightly blueshifted relative to the photoluminescence, with a maximum at ~ 502 nm rather than the 518 nm seen in the PL.

The electroluminescence of the pristine NPPE LED is shown overlaying its photoluminescence in Figure 3.5, showing their similar spectral shape, and that the emission for both appears to be dominated by excimers. There appears to be no easy explanation for why the pristine NPPE LED's electroluminescence is blue-shifted relative to the photoluminescence, especially since it is behaving differently from the pristine DPPE LEDs, when both polymers have identical photoluminescence spectra. Blue shifts in EL emission for MEHPPV LEDs have been shown as an effect of spincasting speed, indicating less interchain interactions for films that have been spincast at high speeds, but both DPPE and NPPE LEDs were processed at the same concentration and the same spin speed, so this does not account for the differences in the spectra of the devices.

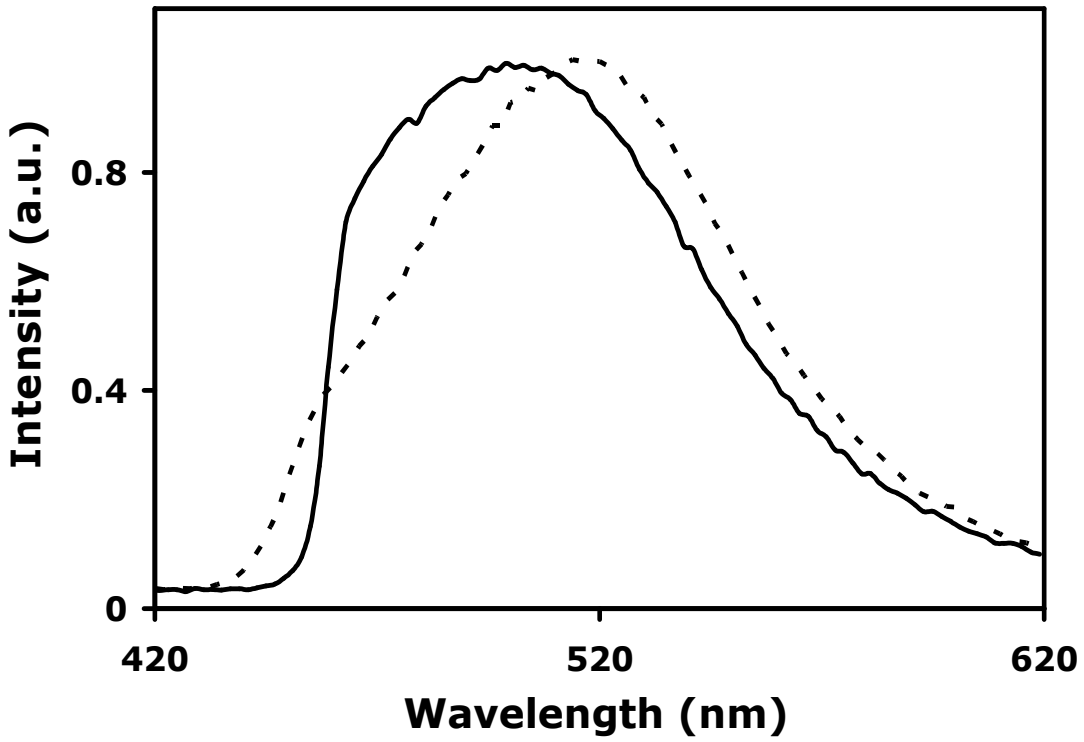

Figure 3.5 Electroluminescence spectrum of a pristine NPPE LED (solid line) overlaid with the photoluminescence spectrum of the same device. Although the EL is slightly blueshifted relative to the PL, both spectra retain the broad, green featureless emission.

NPPE LEDs were annealed in an identical manner to the DPPE devices, with the film briefly heated to a melt (~210 ˚C) then allowed to slowly cool back to room temperature, allowing the polymer chains to rearrange into the preferred lower energy conformation of the ordered domains. The annealed NPPE LEDs also demonstrate birefringence through crossed polarizers, evidence that the films have formed ordered domains, similar to DPPE.

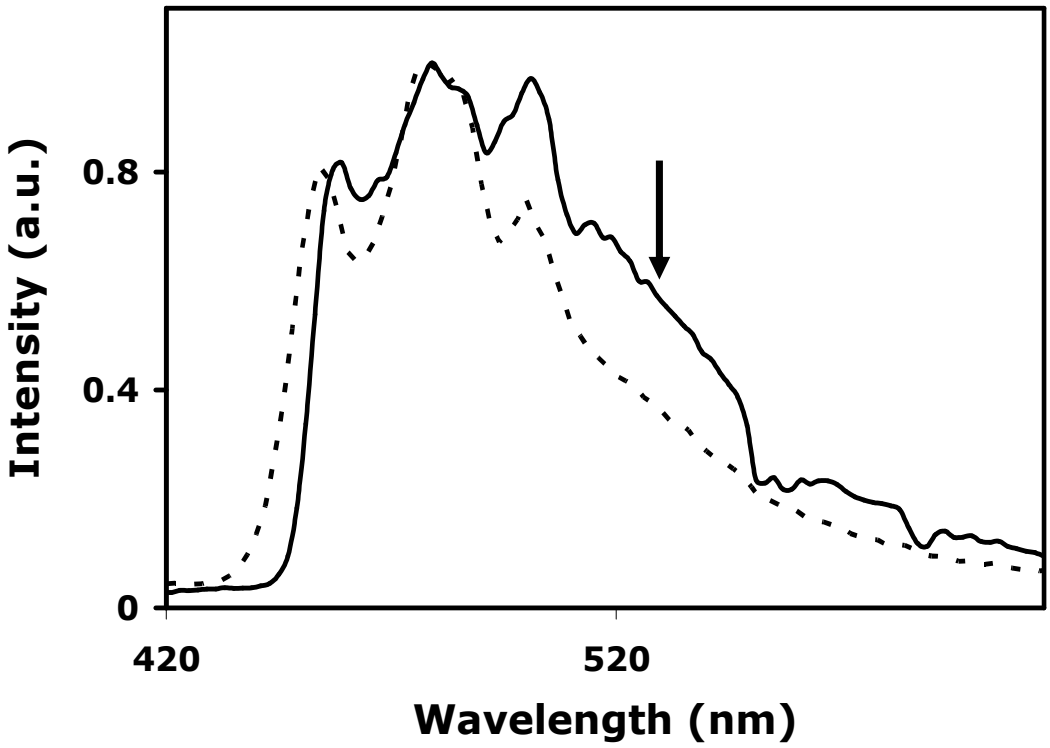

Figure 3.6 Electroluminescence spectrum of an annealed NPPE LED (solid line) and its photoluminescence spectrum (dashed line). The EL is redshifted relative to the photoluminescence, and has a noticeable shoulder marked by the arrow.

Photoluminescence spectra of the annealed NPPE LEDs are identical to the PL of thin films, with no relative shift in the peak maxima. The electroluminescence spectrum of an annealed LED is compared to its photoluminescence spectrum in Figure 3.6. The electroluminescence of the annealed NPPE device is slightly redshifted from the photoluminescence, with its peak maxima at 459 nm, 480 nm and 501 nm, compared to the PL peaks at 454 nm, 478 nm and 500 nm.

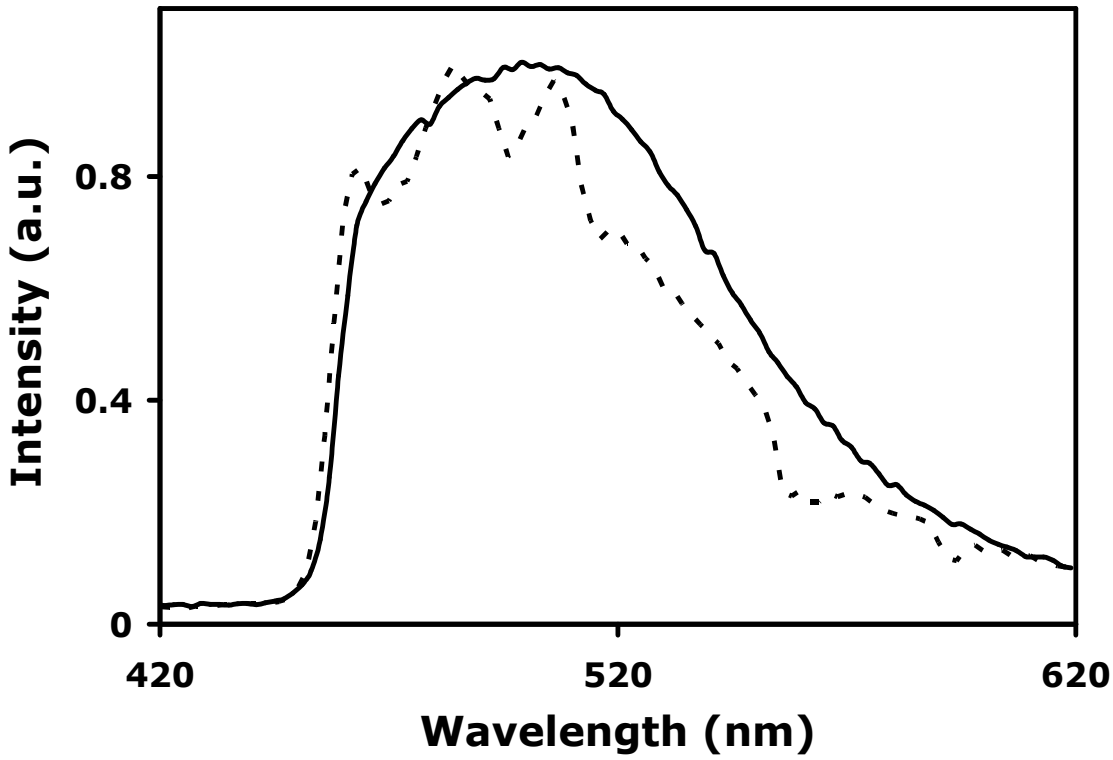

Figure 3.7 EL spectrum of pristine NPPE LED (solid line) and of an annealed NPPE LED (dashed line), showing that both spectra are centered at ~503 nm, even though the annealed device has a more structured emission.

.

In addition to having a redshifted electroluminescence spectrum, there is a noticeable shoulder in the annealed NPPE's EL, with a maximum at ~520 nm, close to the excimer-emission peak in the pristine photoluminescence. Similar to the DPPE electroluminescence spectra, the overlap between the pristine and the annealed NPPE EL spectra is considerable, albeit with the annealed NPPE showing more structure and less of the excimer-based maximum. The overlay of the two EL spectra is shown in Figure 3.7. It appears that for both LEDs, there is a maximum emission intensity favored for electroluminescence where both EL emission spectra are centered: this maximum occurs

for both DPPE EL spectra at ~520 nm, and for both NPPE EL at ~ 503 nm. Since the two polymers have identical fluorescence spectra and devices were prepared and tested under identical conditions, it appears that the only possible explanation is a different packing order between the two films. Since the annealed NPPE electroluminescence appears to have less of the featureless excimer-based emission when compared to the annealed DPPE device, the NPPE film was expected to have a higher degree of order upon annealing, producing fewer of the trapping excimer sites.

NSOM polarization fluorescence anisotropy measurements were taken of the annealed NPPE films in order to determine the amount of polymer order within the film. NSOM polarization anisotropy data has already been published for DPPE, which revealed the well-defined micron-sized domains in the DPPE films had ~ 40% of the polymer aligned in either the horizontal or vertical direction.[7] Thin films of annealed NPPE on glass substrates were examined using NSOM, and the data is shown in Figure 3.8. The x (vertical) and y (horizontal) polarization emission images are shown at the top of the figure, with their respective count intensities normalized. There is correlation between the two polarizations; regions that appear darker in the x-direction appear brighter in the y-direction.

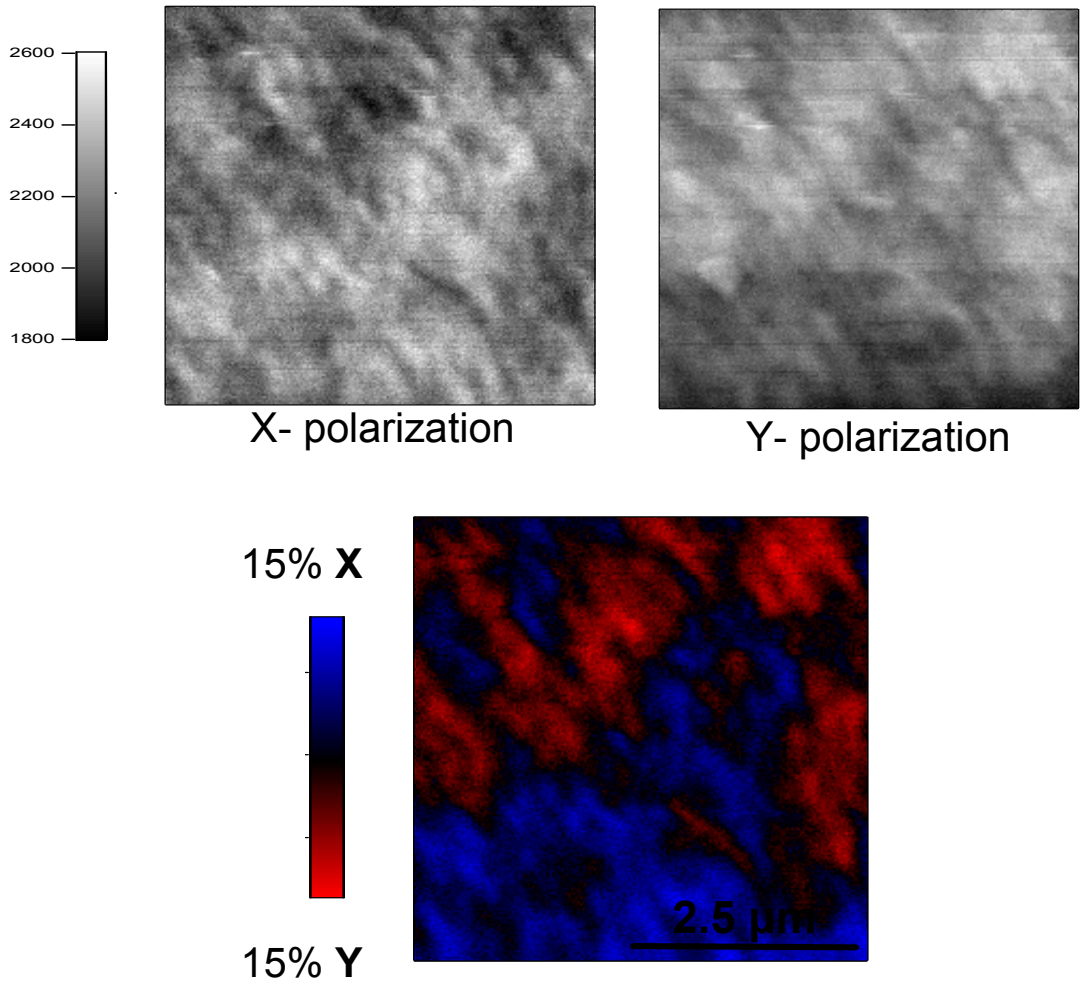

Figure 3.8 NSOM polarization data for an annealed NPPE film. The amount of light polarized in either the horizontal direction (x-polarization) or the vertical direction (y-polarization) is shown at the top of the figure, while the calculated anisotropy over the entire 5 μm scan is shown in at the bottom of the figure, with the calculated percentage of polymer aligned in either direction.

Fluorescence anisotropy was calculated for each pixel and is shown plotted over the entire scan in the bottom of Figure 3.8, showing the domains ordered on the micron-scale similar to DPPE. The percent of polymer aligned in either direction (calculated from an image histogram) was found to be 15%, much less than the 40% order determined for DPPE. Thus there are differences in the two film's morphology, but these differences do the correlate with the dissimilarities seen in the electroluminescence spectra, it is possible that there are other morphological differences, only beneath the resolution of the NSOM instrument.

AFM topography scans were taken of NPPE films, to compare previous topography data shown for DPPE films. Pristine NPPE films have a rough, disordered surface with very small chunks of undissolved polymer seen in the 5 μm scan size. In addition to these small chunks, there are considerably larger chunks of polymer across the film, too large to image sufficiently. Figure 3.9 shows the topography of a NPPE film on glass prior and after annealing, and the topography of an annealed DPPE film on the same size scale. There is some change in the NPPE film after annealing, as the topography appears to have a larger grain size of the surface with increased roughness. However, there are differences in the morphology between the annealed NPPE film and the annealed DPPE film, as the DPPE film exhibits a more crystalline structured surface, with the polymer film forming large, broad clusters of aggregated polymer. NSOM fluorescence scans over the smaller clusters in these films showed decreased fluorescence relative to the rest of the film. These physical polymer aggregates which appear to be more prevalent in the DPPE film could contribute to the broad green electroluminescence emission in the annealed film. The lack of these clusters in the NPPE film could explain why there is more of a blue-shifted structured emission in the annealed film, but does not explain why the pristine EL is blue shifted.

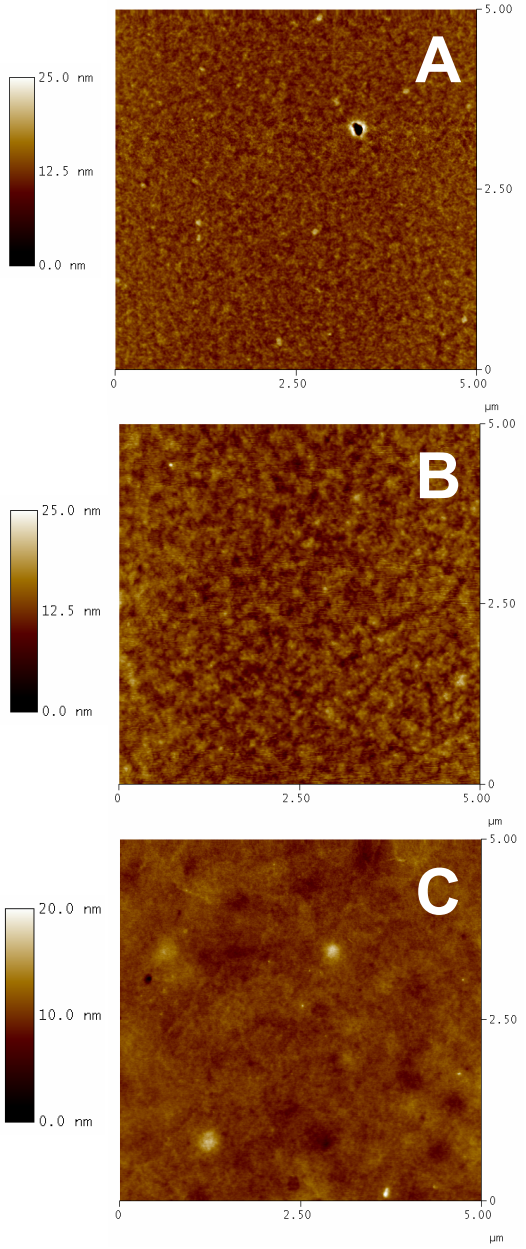

Figure 3.9 AFM topography scans of a pristine NPPE film (A), an annealed NPPE film (B) and an annealed DPPE film (C). There are changes from the pristine NPPE film to the annealed film, but the annealed NPPE film is not as well defined as the annealed DPPE film.

DEVICE CHARACTERIZATION AND COMPARISON

Current-voltage curves and electroluminescence intensity measurements were taken for both types of polymer devices. Turn on voltage varied depending on the processing conditions for the devices, this is covered extensively in Chapter 4. One obvious quality over all of the devices was that the turn on voltage was higher when devices were tested in air; thus all of the measurements in this section were performed in the glovebox for accurate comparisons between devices that had not been exposed to air.

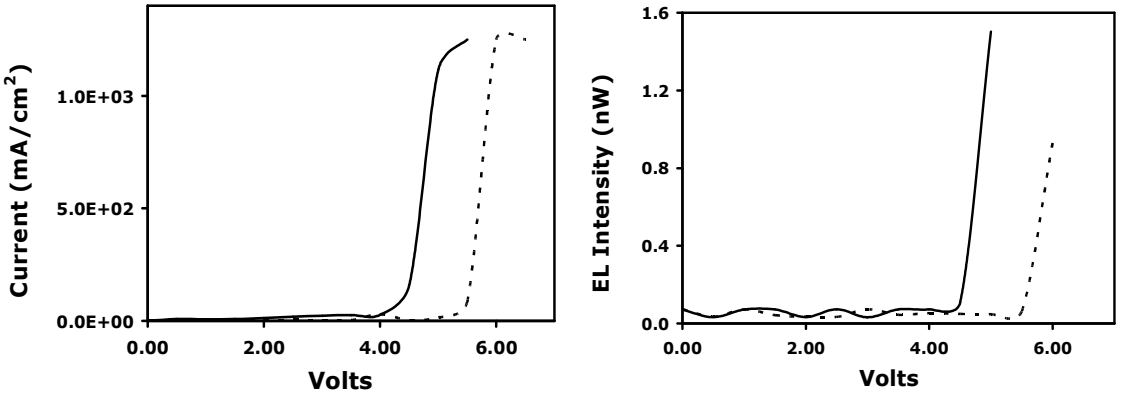

Figure 3.10 Current-voltage and EL intensity curves for pristine (solid line) and annealed (dashed line) DPPE devices, showing the higher turn on voltage for the annealed device and its diminished EL intensity.

Pristine DPPE devices had lower turn on voltages compared to the annealed devices, an example of this is shown in Figure 3.10, along with their respective EL intensities. The turn on voltage was never constant; different processing conditions (along with the inclusion of a PEDOT-PSS layer) would sometimes affect the turn on voltage value, although pristine devices, with few exceptions, had lower turn on voltages and brighter electroluminescence intensities. Within the glovebox, all PPE devices had a

turn-on range between 4-9 Volts. As seen in Figure 3.10, the turn on voltage for the pristine device was at 4. 5 V, while the turn on voltage for the annealed device was at 5.5 V. Also, their electroluminescence intensities follow this trend, with the higher intensity seen for the pristine device at 1.50 nW, compared to the less intense 0.926 nW seen in the annealed DPPE device. It should be noted that these values represent the best values seen for the simple three-layer (ITO-DPPE-Al) devices, but the data consistently produced both higher turn on voltages for the annealed devices in addition to lower EL intensities.

NPPE devices produced in an identical manner to the DPPE devices also exhibited the same traits for pristine versus annealed devices, with higher turn on voltages seen for the annealed devices. The EL intensities for the annealed devices was much closer to the intensity seen for the pristine NPPE devices however, a noticeable difference from the annealed DPPE devices. Current-voltage and EL intensity plots for a pristine and annealed NPPE device is shown in Figure 3.11, showing the differences in the turn on voltage for the two devices, 5.5 V for the pristine NPPE device, and 9 V for the annealed device. The differences in EL intensity for the two devices is slightly less than seen in the DPPE devices; the EL intensity maximum for the pristine device is 1.57 nW, and the annealed device is a slightly lower 1.40 nW. Annealed NPPE devices produced light on a more regular basis than did the annealed DPPE devices. Again, the data in Figure 3.11 is representative of the best data produced, the differences in the two turn on voltages were not always as large, but the annealed devices again were consistently at higher turn on voltages.

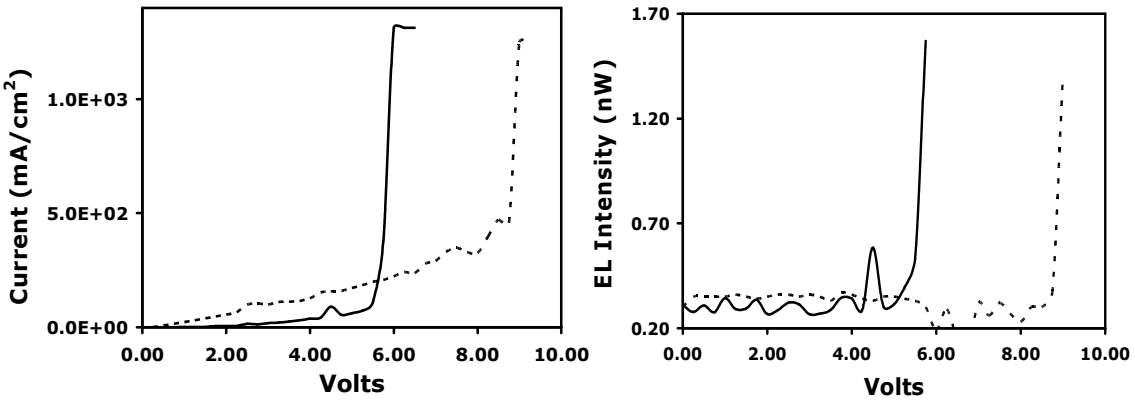

Figure 3.11 Current-voltage and EL intensity curves for pristine (solid lines) and annealed (dashed lines) NPPE LEDs, showing higher turn on voltage for the annealed device, and its only slightly lower intensity in EL.

The difference in the EL intensities for the two devices correlates with the differences seen in their EL emission spectra. The DPPE devices, dominated by the red-shifted excimer emission, do not produce the same level of intensity as the annealed NPPE devices, this was confirmed through visual inspection, as the annealed NPPE devices would light up more brightly over the active area than the annealed DPPE devices. The fewer polymer chain interactions seen in the blue-shifted EL of the NPPE devices resulted in brighter device emissions, indicating that the more excimer-dominated emission seen in the longer sidechain DPPE inhibits efficient light emission.

CONCLUSIONS

Di-alkyl polyphenylene ethynylenes exhibit broad, excimer-based fluorescence as pristine films; which blue-shifts and becomes more structured to resemble a single-chain type of emission after thermal annealing. Annealed di-alkyl PPE films are highly birefringent, and confirmed by NSOM studies, show highly increased order after

annealing. The similarities in the two polymers' fluorescence spectra do not correlate with their electroluminescence spectra; this could be due to small discrepancies between the morphology of the films, as the shorter sidechain NPPE does not order nearly as well as the longer sidechain DPPE, evidenced in NSOM fluorescence anisotropy measurements and AFM topography. These morphological differences do not easily explain the difference in EL spectra for the two polymers, since the DPPE is dominated by an excimer-based EL in both the pristine and annealed form, whereas the NPPE has more of the structured single-chain emission seen in the annealed EL, so the differences must be beneath a detectable limit. The excimer-dominated emission seen in both DPPE EL spectra limits the electroluminescence intensity for the annealed DPPE device, as there are fewer excimer sites in the well ordered annealed film, and efficient exciton recombination occurs preferentially at these low-energy sites. The annealed NPPE devices on the other hand, less dominated by that excimer emission, have exciton recombination occurring at more than just a few excimer sites, producing greater electroluminescence intensities. The degree of order within these films have a large effect on where exciton recombination occurs, showing that the removal of some of the low-energy trap sites do not result in a more productive device, but rather in decreased electroluminescence.

EXPERIMENTAL

Polymers and Characterization All polymers used were provided by Bunz et al. and used without further purification. Average molecular weight of the polymers were determined using GPC (data provided by Bunz et al.); EPPE had an average MW of 9,300 with a polydispersity of 2.6, NPPE had an average MW of 20,300 with a

polydispersity of 3.15, and DPPE had an average MW of 23,000 with a polydispersity of 2.5. Polymer solutions of 0.5% (w/w) polymer in chloroform solution were heated to clarity, then spincast (1000 rpm, 60 seconds in the glovebox) to produce films of 80-100 nm thickness, as measured by a Digital Instruments Multimode AFM in tapping mode. Annealing of the films was performed by briefly heating the film to a melt on a hotplate, then allowing it to slowly cool back to room temperature.

Fluorescence and electroluminescence spectra were taken using a Photon Technologies International Quanta Master model C, using 400 nm excitation light and collecting past 420 nm, with a long pass filter of 418 nm for fluorescence spectra, while the electroluminescence spectra were collected with the excitation lamp turned off to avoid PL contamination of the spectra. NSOM fluorescence anisotropy was collected on an Aurora II system (Thermomicroscopes/Veeco) using NSOM probes purchased from Veeco with apertures in the range of 50-150 nm diameter. Excitation light for NSOM measurements was at 400 nm, using a frequency doubled Ti-Sapphire laser beam, with filters to remove residual 800 nm light before the light entered the NSOM tip, and with 400, 420 nm longpass filters in front of the detectors to remove excitation light. A polarizing beam splitter cube was used to split the fluorescence signal into the horizontal and vertical directions (along/perpendicular to the direction of the sample scan), which were collected on an avalanche photodiode (APD), purchased from EG&G, for the y-direction, and on a microphoton device (MPD), purchased from Picoquant, for the x-direction. The counts for each direction were normalized, as the MPD detector has a smaller window relative to the APD and collects fewer counts as a result. Anisotropy was calculated at each pixel, using Equation 3.1, where Intensity (x) is the vertical polarization and Intensity (y) is the horizontal polarization. This calculates the difference in the polarized emission between the two detectors and divides it by their sum at each

pixel, which is then plotted as the anisotropy. A histogram of the entire image is built up, showing the distribution of the calculated values, this histogram determines the percentage aligned in either direction.

Current-voltage scans were collected using a Keithley 2400 using the two wire resistor configuration. Electroluminescence intensity was measured using a calibrated photodiode (Newport 1830-C) with the selected wavelength as the maximum intensity seen in the EL spectra (503 nm for NPPE, 520 nm for DPPE), collected by the Keithley in the four terminal device configuration for simultaneous current-voltage collection. Current was measured in amps, EL intensity in Nano watts (as shown by the photodiode); current was converted into mA/cm^2 values, to take into account the size of the device.

$$\text{Anisotropy} = \frac{\text{Intensity (x)} - \text{Intensity (y)}}{\text{Intensity (x)} + \text{Intensity (y)}}$$

Equation 3.1 Anisotropy calculation for NSOM polarization fluorescence anisotropy.

LED Fabrication. Single face indium tin oxide (ITO) coated glass slides (4-8 , Delta Technologies) were selectively etched using hot aqua regia solution to remove portions of ITO, then cleaned using an oxygen plasma (March CS1701F RIE etching system, 300 mTorr, 250 W, 35 sccm oxygen, 10 min) to enhance conductivity of the ITO and decrease surface roughness.[27-29] On some devices, a thin (40nm) layer of PEDOT-PSS (Aldrich) was spincast (0.25% w/w in water, 2000 rpm) onto the ITO before application of DPPE. The PEDOT-PSS was not found to inhibit film order or function. The 0.5% (w/w) PPE polymers in chloroform solution were spincast (1000 rpm, 60

seconds) onto cleaned ITO substrates to produce ~100 nm thin films. An aluminum cathode of 200-300 nm thickness was thermally evaporated onto the polymer film using a mask to form an active area ~ 8 mm^2 for devices tested in the glovebox, and ~ 4 mm^2 for devices used to collect electroluminescence spectra, due to the configuration of the photodiode detector in the glovebox, the larger active area was necessary. Annealed films were heated briefly above the melting temperature (150 ˚C for DPPE, and 210 ˚C for NPPE), then allowed to slowly cool back to room temperature. All devices were prepared in a glovebox, IV and EL intensity data were collected within a glovebox, EL spectra were collected under ambient conditions.

REFERENCES

1. Breen, C. A.; Tischler, J. R.; Bulovi , V. and Swager, T. M. *Adv. Mater.* **2005**, *17*, 1981.

2. Tada, K.; Onoda, M.; Hirohata, M.; Kawai, T. and Yoshino, K. *Jpn. J. Appl. Phys.* **1996**, *35*, L251.

3. Montali, A.; Smith, P. and Weder, C. *Synth. Met.* **1998**, *97*, 123.

4. Breen, C. A.; Rifai, S.; Bulovi , V. and Swager, T. M. *Nano Lett.* **2005**, *5*, 1597.

5. Pschirer, N. G.; Miteva, T.; Evans, U.; Roberts, R. S.; Marshall, A. R.; Neher, D.; Myrick, M. L. and Bunz, U. H. F. *Chem. Mater.* **2001**, *13*, 2691.

6. Swager, T.M.; Gil, C.J. and Wrighton, M.S. *J. Phys. Chem.* **1995**, *99*, 4886.

7. Bunz,U.H.F.; Imhof, J.M.; Bly, R.K.; Bangcuyo, C.G.; Rozanski, L.J. and Vanden Bout, D.A. *Macromolecules* **2005**, *38*, 5892.

8. Kim, Y.; Bouffard, J.; Kooi, S.E. and Swager, T.M. *J. Am. Chem. Soc.* **2005**, *127*, 13726.

9. Liu, C. P. and Hung, Y. T. *Thin Solid Films* **2005**, *492*, 269.

10. Niu, Y-H.; Hou, Q. and Cao, Y. *Appl. Phys. Lett.* **2002**, *81*, 634.

11. Ahn, T.; Lee, H. and Han, S-H. *Appl. Phys. Lett.* **2002**, *80*, 392.

12. Zyung, T.; Jung, S.-D. and Hwang, D.-H. *Synth. Met.* **2001**, *117*, 223.

13. Lee, T-W. and Park, O. O. *Adv. Mater.* **2000**, *12*, 801.

14. Cornil, J.; dos Santos, D.A.; Crispin, X.; Silbey, R. and Bredas, J.L. *J. Am. Chem. Soc.* **1998**, *120*, 1289.

15. Blatchford, J. W.; Jessen, S.W.; Lin, L.B.; Gustafson, T.L.; Fu, D.K.; Wang, H.L.; Swager, T.M.; MacDiarmid, A.G. and Epstein, A.J. *Phys. Rev. B* **1996**, *54*, 9180.

16. Schmitz, C.; Pösch, P.; Thelakkat, M.; Schmidt, H.W.; Montali, A.; Feldman, K.; Smith, P. and Weder, C. *Adv. Funct. Mater.* **2001**, *11*, No. 1, 41.

17. Ding, L.; Lu, Z.; Egbe, D. A. M. and Karasz, F. E. *Macromolecules* **2004**, *37*, 10031.

18. Kim, T-H.; Im, S. H.; and Park O. O. *Appl. Phys. Lett.* **2005**, *87*, 221114.

19. Niu, Y-H; Hou, Q. and Cao, Y. *Appl. Phys. Lett.* **2003**, *82*, 2163.

20. Huang, Y.; Lu, Z.; Peng, Q.; Jiang, Q.; Xie, R-G.; Han, S-H.; Dong, L.; Peng, J-B.; Cao, Y. and Xie M-G. *Mater. Chem. And Phys.* **2005**, *93*, 95.

21. Jandke, M.; Strohriegl, P.; Gmeiner, J.; Brütting, W. and Schwoerer, M. *Adv. Mater.* **1999**, *11*, 1518.

22. Chung, S-J.; Kwon, K-Y.; Lee, S-W.; Jin, J-I.; Lee, C. H.; Lee, C. E. and Park, Y. *Adv. Mater.* **1998**, *10*, 1112

23. Jiang, G.; Wu, J.; Yao,Y.; Geng, Y.; Cheng, Y.; Xie, Z.;Wang, L.; Jing, X. and Wang, F. *Macromolecules* **2006**, *39,* 7950.

24. Luo, J.; Peng, J.; Cao, Y. and Hou, Q. *Appl. Phys. Lett.* **2005**, *87*, 261103.

25. Zhou, X-H.; Zhang, Y.; Xie, Y-Q.; Cao, Y. and Pei, J. *Macromolecules* **2006,** *39,* 3830.

26. Lee, P-I.; Hsu, S. L-C. and Chung, C-T. *Synth. Met.* **2006**, *156*, 907.

27. Kim, J. S.; Granström, M.; Friend, R. H.; Johansson, N.; Salaneck, W. R.; Daik, R.; Feast, W. J. and Caciallia, F. *J. Appl. Phys*. **1998**, *84*, 6859.

28. Xue, J. and Forrest, S. R. *J. Appl. Phys.* **2004**, *95*, 1869.

29. Chan, I-M. and Hong, F. C-N. *Thin Solid Films* **2003**, *444*, 254.

CHAPTER 4: PRODUCTION AND TESTING OF PPE SANDWICH-TYPE LIGHT EMITTING DEVICES (LEDS)

BACKGROUND

The production of light emitting devices (LEDs), also referred to as light emitting diodes, is known as a black art, and there is extensive research on perfecting production techniques to improve device performance. Polymer-based LEDs (PLEDs) have an advantage over their small organic molecule-based counterparts, OLEDs, due to their lower production costs and applicability towards flexible devices. However, PLEDs have been plagued by lower quantum efficiencies, shorter device lifetimes, higher turn on voltages and fluorescence color purity problems in comparison to OLEDs,[1-4] leading to the large quantity of research put forth. How well the device functions is directly related to its fabrication, with two main factors inhibiting electroluminescence from PLEDs: charge injection and charge transport. The former relates to the HOMO and LUMO levels of the polymer relative to prospective electrodes, with the differences in workfunctions a barrier to injection, as well as the degree of contact made between the polymer film and the electrodes, while the latter depends on the conductivity of the polymer itself, which is affected by the morphology of the film.[5-8]

To correct for the charge injection limitations, considerable research has gone into matching work functions of the polymer to the electrodes, primarily through modification of the commonly used anode, ITO, or through the addition of transition layers between the polymer film and electrode that lowers the energy barrier.[9-15] Figure 4.1 shows a simple illustration of the relative energy levels for the two electrodes used in the PPE-PLED compared to the HOMO and LUMO levels for PPE.[16] As seen in the figure, ITO often has a lower work function compared to the HOMO level for many conjugated

polymers. One popular way to both increase this work function and enhance device performance is through plasma treatments of the ITO surface, with literature supporting plasma treatments using argon gas, oxygen gas, CF_4 gas or combinations of these gases.[9-11,17-19] Acid or base cleaning treatments have been utilized to smooth the ITO surface without changing the work function of the ITO, or have been combined with the plasma treatments to produce devices with higher efficiencies.[17, 20-21] Arguments for why the various plasma treatments are effective have been: argon cleans the surface and decreases the amount of tin, oxygen injected into the ITO increases the conductivity, as does fluorine injected into the ITO from the CF_4 plasma.[17-18] The surface roughness does not seem to directly affect the work function of the ITO, but instead it can lead to the formation of shorts within the device, as the sharp, tall points of ITO can pierce through the polymer to the cathode.[22]

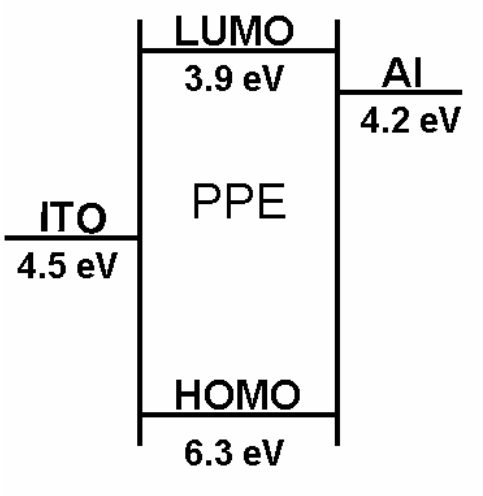

Figure 4.1 Diagram of relative work function levels for the electrodes compared to the HOMO and LUMO levels of PPE.

In addition to cleaning and changing the work function of the ITO anode, the insertion of a hole-transport material such as PEDOT-PSS has been found to improve device function.[13,22-23] Other materials have been used in place of PEDOT-PSS, but for these studies only PEDOT-PSS was examined, as it was an inexpensive, simple material to use, and has been well examined in the literature. The semiconducting polymer PEDOT is positively charged, and has been mixed with a negatively charged PSS matrix so that thin films could easily be applied on ITO through spincasting from solution. Various treatments have been applied to the PEDOT-PSS films in order to improve the film's conductivity, further enhancing the charge injection into the polymer.[12,24]

Improvements to electron injection from the metal cathode have also been employed to great success. Most of the popular conjugated polymers used in LEDs are primarily hole-transport materials, with extremely low LUMO levels, usually around 2-3 eV, meaning that an aluminum cathode, with its work function of 4.2 eV, would inject electrons very poorly if at all; thus many researchers switched to using metals such as calcium or magnesium, with considerably lower work functions than aluminum.[25] Since these metals are not stable in air, a capping layer of aluminum was added for stability. Unfortunately, it has been shown that the low-work function metals diffuse into the polymer film during deposition, ultimately making the polymer insulating.[26] However, as was seen previously for alkoxy-PPE LEDs,[27] the low work function metals did not improve PPE device efficiency at all, indicating that there was a good match of energy levels between aluminum and the polymer, as shown in the diagram of Figure 4.1.

Others have improved electron injection from the metal cathode by the insertion of a very thin (~1-2 nm) insulating layer of lithium fluoride, LiF. There are numerous theories as to why this extremely thin insulating layer improves the device function, including: (1) the layer improves tunneling of electrons into the polymer layer, (2)

dissociation of lithium and fluoride ions blend into the film, enhancing its conductivity, (3) LiF provides protection of the polymer film from thermal damage as the aluminum cathode is evaporated, and (4) the LiF layer dipole aligns along the metal electrode, lowering its effective work function.[14,25] Recent papers have examined using sodium hydroxide or sodium chloride as a inexpensive or non-toxic alternatives to LiF, with reported success.[28-29]

Besides controlling parameters of both electrodes, the morphology of the polymer also plays a large role in how a device functions, as seen in Chapter 3 on the PPE devices. Besides the thermal treatments of the polymer devices, other attempts at affecting the morphology, through changing the solvent used, the solution concentration or spincasting speed of the films were not performed. Interest in the device function of PPEs was focused on the effects between increased film order from thermal annealing on exciton migration within the films.

A final aspect not mentioned in the literature is the importance of active area size towards producing working devices. Larger active areas increase the likelihood of encountering surface defects, either on the electrodes or within the polymer film that can short out an entire device. Thus smaller active areas, ranging from 4-8 mm^2, with multiple active areas per device are preferable for testing. Conducting nanoscale AFM studies on ITO surfaces have also shown conducting and non-conducting regions at the ITO surface, with a large amount of heterogeneity of current injection from the ITO surface;[30] so devices were redesigned to have a large continuous ITO anode with small multiple aluminum cathodes on each device. The large ITO anode is believed to allow for multiple pathways along the conducting areas dispersed throughout the non-conductive areas of the ITO for increased current flow from the voltage source to the small active areas. The device configurations are illustrated in Figure 4.2, showing the

various changes in device setup as improvements were made. The initial setup, shown in A, did not produce many working devices, while the device B improved the number of emitting devices, but suffered from a lack of multiple active areas per electrode. Due to the setup used in current-voltage and EL intensity measurements, device B was used for these experiments for both types of PPE devices. The setup in C produced the greatest number of working electrodes, due to the number of active areas on each device. Electroluminescence spectra were collected from devices in the C configuration.

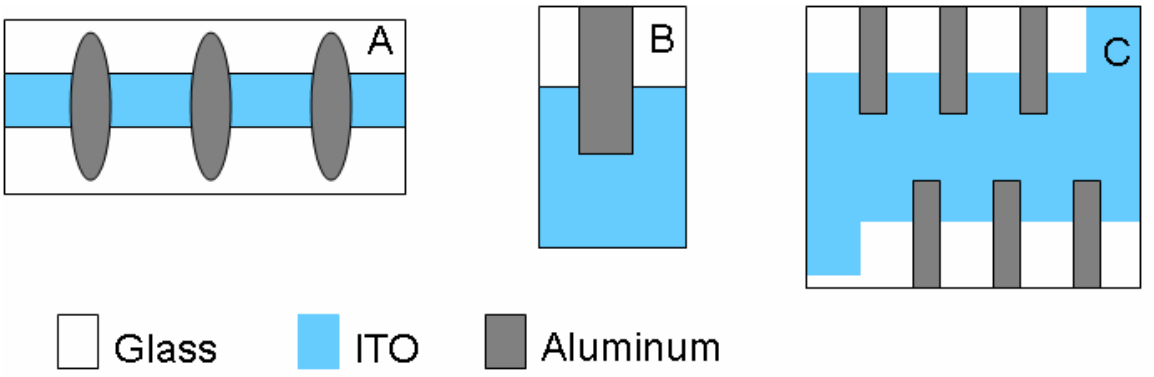

Figure 4.2 Diagrams of the PPE devices used, (A) initial setup with three active areas per device, (B) larger ITO surface, improved function over (A), but limited active areas, and (C) final device configuration, with multiple active areas and large ITO anode.

For the purposes of this chapter, non-working devices are defined as devices that either showed current and no light emission, or showed current flow with only brief flashes of light emission, insufficient to collect for an EL intensity curve or spectrum. For working devices, it was seen that multiple runs on the same device decreased the light intensity electroluminescence; this occurred for both pristine and annealed devices. Increasing the voltage for devices, even after multiple runs, would increase the EL

intensity, but there were fluctuations in this intensity value for all devices as voltage was either ramped up or held at a single value.

PREPARATION AND TESTING OF THE ITO ANODE

For the most efficient hole injection into the polymer film, plasma treatment of the ITO serves two functions- removing contamination from the ITO surface and lowering its work function. The ITO used for our PPE LEDs was purchased from Delta Technologies, at the lowest resistance available, 4-8 , on either polished float glass (higher surface roughness) or on aluminosilicate glass (lower surface roughness). AFM images of the untreated ITO surfaces for both films revealed that they had very different structure- the float glass substrate had smaller grains of the ITO, while the aluminosilicate glass substrate had considerably larger, flatter grains of ITO, shown in Figure 4.3. All AFM images were obtained using a Digital Instruments Multimode AFM. Both ITO samples had very sharp high peaks of ITO, with the "smoother" ITO sample having a greater concentration of these high peaks. For each film, the high points measured ~30-50 nm, high enough that they could contribute to shorts within a device, this was part of the reason pristine ITO substrates were not used for devices. The surface roughness of the film, calculated using the NanoScope AFM software, was 4.906 nm for the ITO on aluminosilicate, and 4.758 nm for the ITO on float glass, both for 10 μm scan sizes. The higher roughness on the "smoother" ITO is due to the multiple sharp spikes on the surface. For a comparison to further plasma treatments, AFM topography scans are shown for the two untreated ITO samples in Figure 4.3, showing the difference in the ITO grain size.

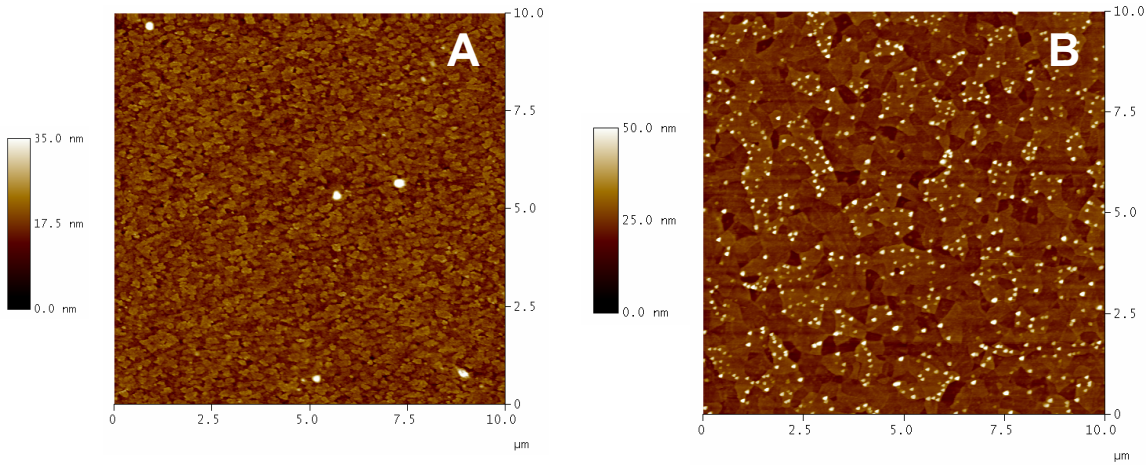

Figure 4.3 AFM topography scans of untreated ITO on float glass (A) and on aluminosilicate glass (B).

An oxygen plasma treatment was initially chosen as it appeared to give some of the best results in the literature, with plasma cleaning of substrates performed in a March Plasma CS1701F RIE etching system. A table of the various treatments and their results is shown in Table 4.1; oxygen plasma, argon plasma and CF_4 plasma, or combinations thereof have been shown as very successful in the literature, [9-11,17-19] and were combined with acid or base treatments to further remove the high, sharp ITO peaks. Using identical parameters to what was listed in the various literature did not produce identical results, for example, the best parameters given by Kim et al. using 100 % oxygen (assumed to be 100 sccm, as no value was given) at 400 W for 10 minutes produced considerably rougher ITO surfaces which performed poorly as devices. All plasma treatments were performed on ITO films that had been rinsed with methanol and dried briefly in an oven; multiple sonications of ITO samples in various solvents, as often listed in the literature, did not produce any differences of the ITO surface after plasma treatment compared to samples rinsed only in methanol.

Many papers did not include the full range of information needed; sometimes the amount of gas or the pressure in the plasma chamber was left out, so these parameters were filled in based on what was used in other literature. The oxygen plasma was explored in depth, with some of the choices used shown in Table 4.1 (others lacked characterization besides device performance and were not included). High sccm values of oxygen did not improve device performance; a concentration 30-35 sccm produced the most devices with light emission. The power value was also an important factor, with a range of 200 watts to 300 watts combined with 30-35 sccm oxygen as having the best result. Power values had to be gradually lowered over the course of the experiments due to metal contamination from the RIE plasma cleaner which showed up as a shiny black film along the edges of the ITO; switching the power levels from 300 to 250 W prevented contamination without sacrificing the desired surface structure. The very high power value of 400 W, considered to be the best by Kim et al. (a thoughrough review),[17] produced considerably rougher surfaces, larger than the roughness of the untreated ITO films, and most likely contributed to shorts within the thin PPE films, as the higher power samples tended to have excellent current flow and no light emission. The pressure in the plasma chamber was not found to have much of an effect on the substrates, however a minimum pressure of 200 mTorr was used as lower pressures prevented the plasma formation. Ten minute exposure times were used for all of the samples listed in Table 4.1 with the exception of the O_2/CF_4 and O_2/Argon plasmas, which used shorter times provided in the literature.[11,18] Shorter exposure times did not produce working devices, so ten minutes was kept as the standard.

Since the high peaks on the ITO surface have been shown to contribute to shorts in LEDs, plasma treatments were used after a dilute acid wash (12 H_2O: 3 HCl : 1 HNO_3) for 5 minutes,[31] or after a base soak (sat' KOH/ Isopropanol Alcohol) overnight,[21] with

results for both shown in Table 4.1. The acid, by itself or combined with plasma, produced extremely smooth ITO surfaces, but still left behind a small number of the undesired ITO high peaks. Neither of the acid treatments produced light-emitting LEDs. Base-treated ITO fared better, with no high ITO peaks seen in any of the 10 μm scans taken. LEDs produced from the base-treated then plasma cleaned substrates did not produce many working LEDs; those that did have light emission had an erratic current that would increase, decrease, and increase again, but when light was produced, it occurred at much lower current densities compared to the oxygen-plasma cleaned devices. These devices did not produce brighter electroluminescence or lower turn on voltages compared to samples treated only with the oxygen plasma.

Plasma	**Percent Gas**	**Power**	**ITO Roughness**	**Result**
O_2	30 sccm	300W	2.374 nm	Excellent
O_2	30 sccm	400W	6.543 nm	Poor
O_2/ CF_4	10:10 sccm	100 W	2.691 nm	Poor
acid/O_2	100 sccm	150W	2.071 nm	Poor
acid	N/A	N/A	1.697 nm	Poor
base/O_2	50 sccm	200W	2.063 nm	Average
O_2+ Argon	50 :30 sccm	100 W	2.122 nm	Poor
Smooth ITO				
oxygen	35 sccm	300 W	2.452 nm	Excellent
oxygen	35 sccm	400 W	10.519 nm	Poor

Table 4.1 Summary of various ITO treatments examined by AFM topography measurements, showing the relative roughness of the treated substrates, and how the LEDs produced using these treatments performed.

Figure 4.4 shows AFM topography scans of (A) the best oxygen-plasma cleaned ITO (30 sccm, 300 W, 300 mTorr, 10 minutes), and (B) the base-soaked then plasma cleaned ITO substrate (50 sccm, 200 W, 300 mTorr, 10 minutes). The surface of the oxygen-only prepared ITO is smoother than the plain ITO, while the surface of the base-cleaned sample shown in (B) is considerably smoother.

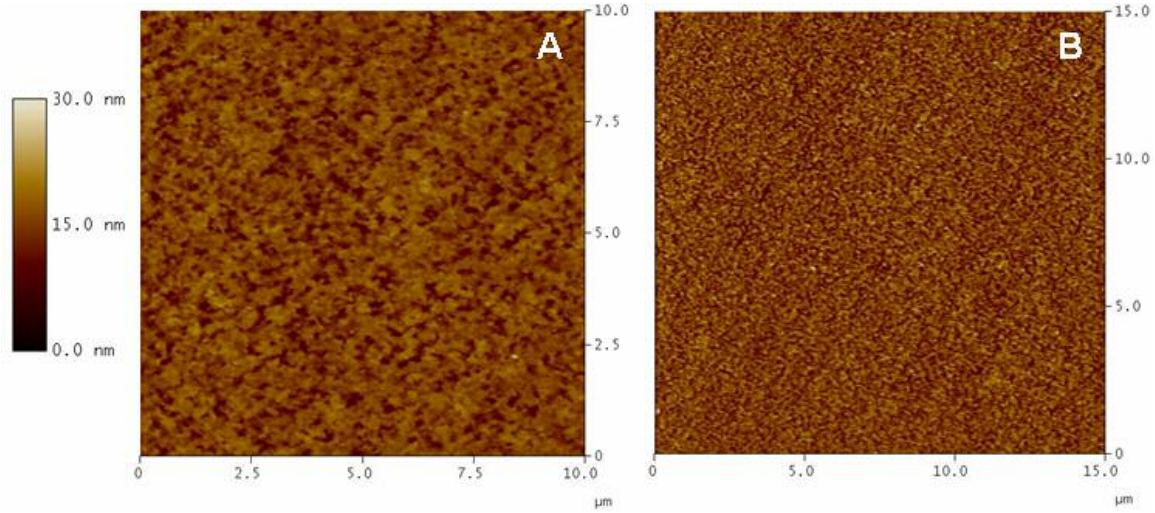

Figure 4.4 AFM topography of the preferred oxygen-plasma treated ITO surface (A), and of a very smooth base-soaked then oxygen-plasma cleaned ITO surface (B), illustrating that more than surface roughness affects device function.

The injection efficiency of ITO into polymer films depends on multiple parameters, including the concentration of different species on the ITO surface (various tin oxides, indium oxides, and metallic indium and tin), the amount of crystalline and amorphous phases of ITO on the surface,[32] and carbon or other contaminants on the surface.[17-19] Plasma cleaning should remove the majority of any contaminants adsorbed to the surface, so the base treatment must affect how the oxygen-metal species are formed, or possibly etches more of the conductive amorphous ITO areas, decreasing the work function.

The smooth ITO on aluminosilicate glass purchased from Delta Technologies, with its considerably larger grain size of ITO on the surface, on average did not perform any better than the small grain size, inexpensive ITO. Similar to the ITO on float glass, oxygen plasma treatments were performed on the substrates (Table 4.1) and AFM

topography images were obtained in order to examine roughness and compare it to samples on float glass. The smooth ITO had a slightly higher surface roughness compared to the ITO on float glass, although the appearance of the film is smoother due to the larger, flat ITO grains. AFM topography images of this ITO cleaned by oxygen plasma at 300 W compared to one cleaned at 400 W is shown in Figure 4.5. The higher power sample created deep holes and peaks in the topography, accounting for the high degree of roughness listed in Table 4.1; while the film cleaned at the lower power smoothed the edges of the grains without completely removing the small high peaks of ITO, seen as small white dots in the AFM image (A). The little difference between final surface roughness of the ITO films and overall device performance between the ITO samples on float glass or aluminosilicate glass indicates that the grain size of the ITO is not as important to device function as the final film roughness or change in work function from the plasma treatments, although some of the devices on the ITO/aluminosilicate glass performed better, this was not consistent over a large number of devices tested.

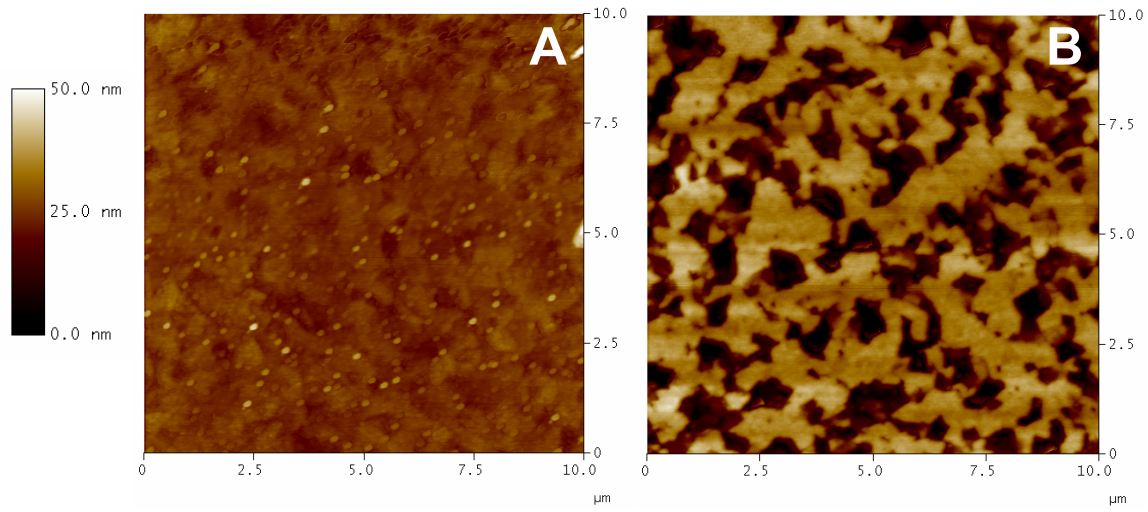

Figure 4.5 AFM topography of ITO on aluminosilicate glass after oxygen plasma cleaning at a power of 300 W (A), and at 400 W (B), showing deep holes produced in the latter film, increasing its surface roughness.

From all of the evidence seen for the different ITO treatments, it is apparent that surface roughness of the ITO does play a part in how well a device will work, since the ITO samples with the largest degrees of roughness performed the most poorly. Surface roughness alone is insufficient for a working device, as the acid and base treated substrates (without further plasma treatment) fared poorly, thus oxygen or similar plasma treatments of the surface are really the best method towards producing better devices. Oxygen plasma alone was chosen for device preparation due to the fact that it initially demonstrated the greatest number of devices that produced EL. Optimization of parameters such as gas concentration, power, and exposure time for other proven plasmas, such as O_2/CF_4, would very likely produce effective working devices as well, but time constraints limited further testing of parameters for these treatments. Even with the preferred oxygen plasma treatment, devices that underwent identical preparation did not always work, often different electrodes on the same device performed differently,

some shorting out, others producing current but no light, and some emitting efficiently, most likely the result of defects within the polymer film or on the surface of either electrode.

MODIFICATION OF ITO ANODE WITH PEDOT-PSS

Poly(3,4-ethylenedioxythiophene) poly(styrenesulfonate), or PEDOT-PSS is a mixture of two polymers, with PSS having some negative charges and the semiconducting PEDOT carrying some positive charges. This was purchased as an aqueous suspension (2.8 % in water) from Aldrich, diluted to 0.25 % in millipure water, filtered through a 450 nm filter and spincast at 2000 rpm to produce ~ 60 nm thick films as measured by AFM. Thin films were then cured in air at 100˚ C for thirty minutes before application of the PPE layer.[29]

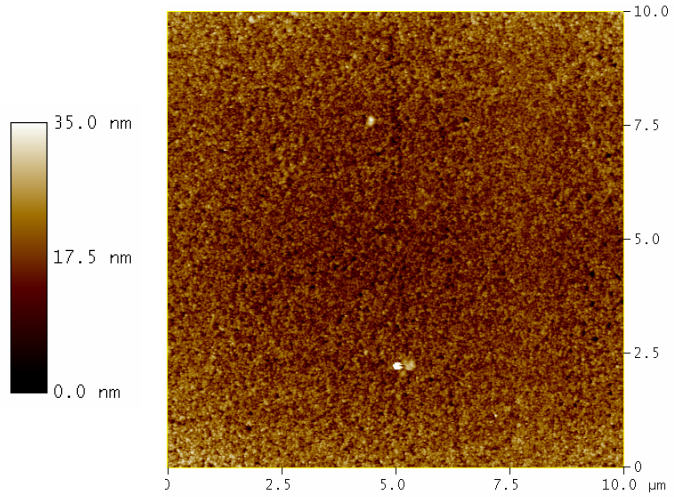

Figure 4.6 AFM topography of PEDOT-PSS film on cleaned ITO, showing the rough appearance of the surface.

The inclusion of the thin PEDOT-PSS layer into devices often lowered the turn on voltage, down to 4-5 V from 6-7 V for annealed DPPE as an example, and often made the device more durable, so multiple runs on one device could be performed without it shorting out. The PEDOT-PSS layer did not appear to affect the ordering of the PPE films upon annealing, nor did it affect the photoluminescence or electroluminescence spectra of these films. Although the inclusion of the PEDOT-PSS increased the overall surface roughness of the film, from 2.374 nm up to 5.856 nm, the surface is fairly even and this increased roughness does not appear to negatively affect the device function. Figure 4.6 is an AFM topography scan showing the morphology of the PEDOT-PSS after it has been spincast and cured on a plasma-cleaned ITO substrate. The surface of the PEDOT-PSS although measured at a higher surface roughness, is believed to create a more even injection of current into the polymer film, so the improvement in devices is through improved hole injection rather than through possible surface effects.

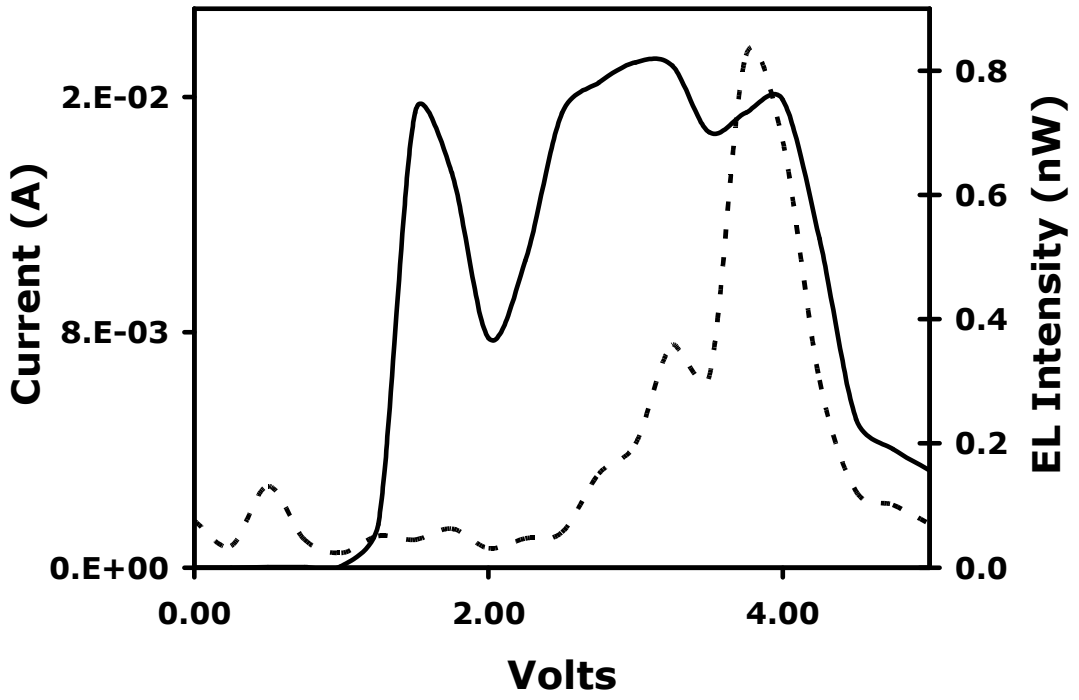

Figure 4.7 Current-voltage and EL intensity curves for a pristine DPPE device containing a PEDOT-PSS layer doped with ethylene glycol, showing the irregularities in the scans.

The EL intensity also increased slightly for some devices, but was not consistent, so data collected for the previous chapter was from the basic LED setup to rule out possible inconsistencies. In order to increase the conductivity of the PEDOT-PSS, an example was taken from the literature: doping the PEDOT-PSS solution with 20 % ethylene glycol, then spreading a thin film of the solution over the ITO and curing briefly with a heatgun.[12] The result was dramatic irregularities seen in the current and EL intensity curves, an example is shown in Figure 4.7, for a pristine DPPE film. These devices tended to have lower turn on voltages combined with lower current values when

light emission was witnessed- in Figure 4.7, the current was 0.02 amps when light was detected, in devices without this layer, the light often shows up at values of 0.08- 0.1 amps. For devices containing PEDOT-PSS alone, as well as devices without any hole transport layer, light intensity increases quickly, directly correlating to the increasing current. Due to these problems in the current-voltage curves, using a film of PEDOT-PSS with ethylene glycol was not continued. As useful as the PEDOT-PSS has been for other devices in the literature, it was ultimately left out of current-voltage studies to rule out any contribution to the electroluminescence intensities or variations in film morphology, considering that light was produced in devices without this layer.

ADJUSTMENTS TO THE METAL CATHODE

Montali et al.'s examination of various cathodes for alkoxy-PPE LEDs was confirmed for the di-alkyl PPEs used in this study by testing LEDs made with a low work function metal, calcium. Similar to what was shown in the literature, a thick, 200 nm layer of calcium was deposited onto PPE LEDs, all other parameters being the same (no PEDOT-PSS, oxygen plasma cleaned ITO), then capped by a thin, 50 nm layer of aluminum.[27] As seen with other poor PLEDs, most of these devices flashed EL briefly in a few spots along the active area before the device shorted out, verifying what had been reported in literature. Calcium did not improve device function, so other low-work function metals were not examined.

Sodium hydroxide, being inexpensive and available, was included as the thin insulating layer for some PLEDs. Controlling the evaporated thickness of the insulator (1-2 nm), was not reproducible, and many devices made with the included layer were shorted out. Visual inspection of a few working devices including this layer revealed that the brightness was definitely improved, thus further optimization of parameters of

this layer, or inclusion of other similar layers, could very well be a viable route towards improving device function. The lack of working devices using sodium hydroxide meant that no data was collected for these samples besides visual inspection.

CURRENT-VOLTAGE AND EL INTENSITY CHARACTERIZATION OF PPE DEVICES

The lack of reproducibility in the PPE devices hindered data collection. Problems with producing working devices was not related to the polymer, as devices were also made using MEHPPV, a very well studied conjugated polymer that is the ideal testing material for PLEDs. The MEHPPV devices behaved in an identical fashion as the PPE devices, having problems such as: current flow but no light emission, brief flashes of light being emitted followed by device failure, and light emission that lasted only briefly or only portions of the active area producing light.

Current flow without light emission was the most common setback in the production of working devices; this was the result of shorts within the film that allowed the current to flow directly between the two electrodes, bypassing the higher resistance polymer film. Without electrons and holes injected efficiently into the polymer film, no excitons were formed, and thus no light emission was produced. The intermittent light emission and the emission seen from only portions of the active area can not be easily explained, but are possibly due to defects in the devices.

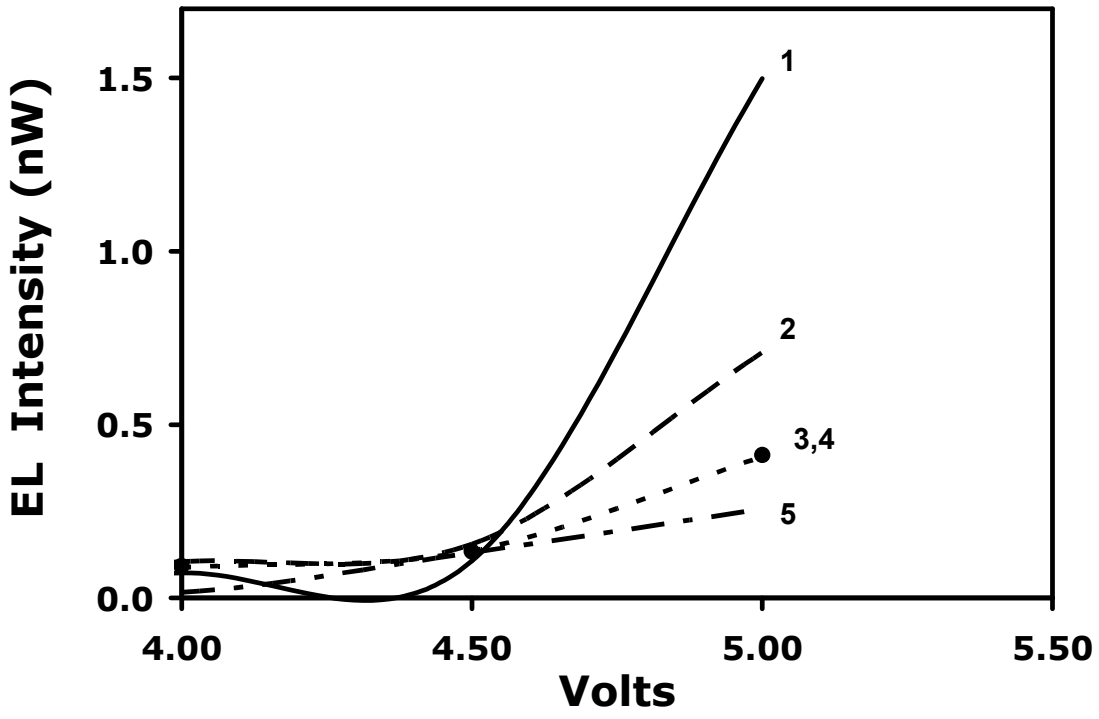

Figure 4.8 EL intensity curves for a pristine DPPE device during multiple voltage scans. The initial scan had the brightest intensity, subsequent scans were decreased, with numbers marking each of the individual scans. Voltage cycles decrease the device efficiency.

Data collected for Chapter 3 was done on the simple three layer LED (ITO:PPE:Al) as these devices demonstrated the most reproducible light emission intensities and current-voltage curves. Multiple voltage sweeps on a single device resulted in a decrease of EL intensity, shown in Figure 4.8. An increase in EL intensity was expected, as cycling of the devices should fill low-lying traps to allow for greater current injection into the film. It is seen in Figure 4.8 that the turn on voltage for electroluminescence has increased slightly for the multiple cycles, the slope of the current-voltage curve (not shown) decreases over the cycles as well, indicating that the

voltage put across the device is causing shorts or some manner of defects within the film that allow the current to bypass the polymer, thus a higher voltage is needed before turn-on.

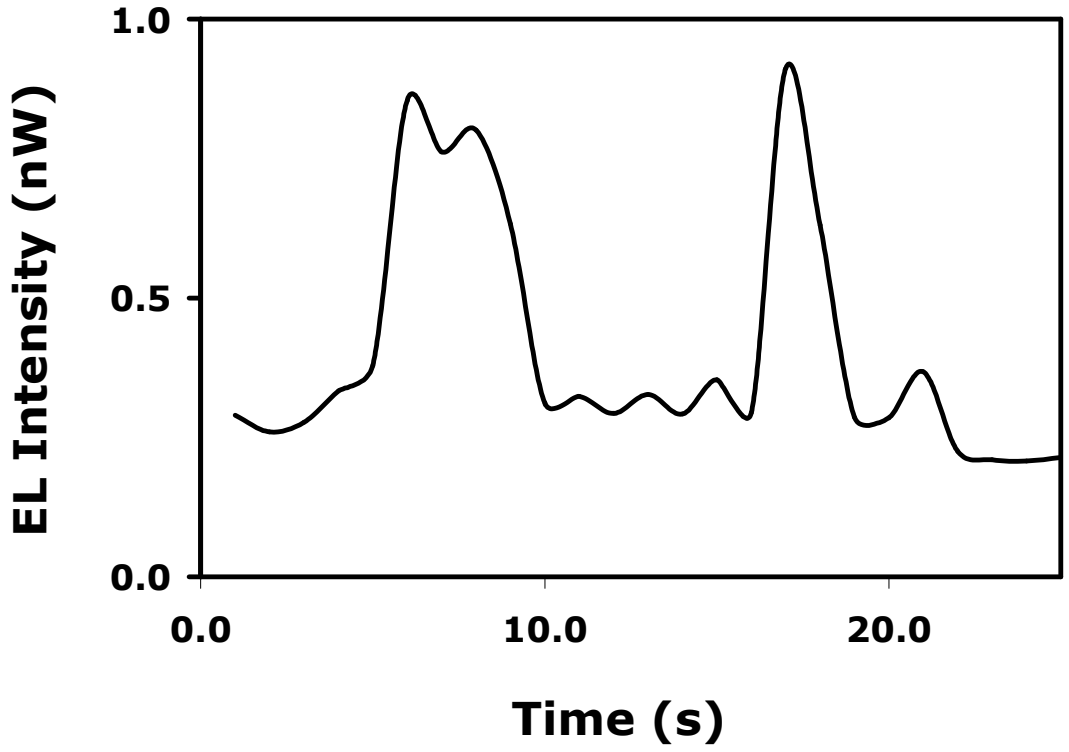

Figure 4.9 EL intensity measured over time for a pristine DPPE device containing a PEDOT-PSS layer, while the voltage is held at 5.5 V. There are large fluctuations in the EL intensity overtime, seen for PPE devices with or without the PEDOT-PSS layer.

Since decreased electroluminescence was seen for multiple voltage cycles across a LED, only initial scans of devices were used for data shown in the previous chapter. The few working devices were fairly stable, and would continue to produce

electroluminescence if the voltage of the device was held constant or steadily increased, although the intensity of EL would fluctuate, as seen in Figure 4.9. These fluctuations occur over all the PPE devices tested, regardless of inclusion of a PEDOT-PSS hole transport layer. These fluctuations were also visible to the naked eye, with the illuminating areas becoming brighter and darker, but not flashing on and off as seen in the dysfunctional devices. Visible fluctuations were not seen for all devices; working devices of the latest iteration of device configuration "C" generally had fully illuminated active areas, with some portions appearing brighter than others, but any fluctuations in EL intensity could not be detected by the naked eye. Time constraints limited further examination of these devices, so EL intensity curves were not obtained.

CONCLUSIONS

For a beginner's approach to preparing working light emitting devices, systematic steps must be taken to ensure proper device function. Considering the magnitude of literature devoted to making improvements on device efficiencies and turn on voltages, sometimes with conflicting results, filtering through the multiple treatments of electrodes and films to determine which of the techniques will work best for a new system is daunting. From the trial-and-error method taken for the PPE-based LEDs, it was discovered that the techniques that have been seen the most often in various papers will work the best, provided some time and effort is spent in optimizing the parameters for a new system. For example, the oxygen plasma treatments of ITO, with dozens of different parameters given in varied papers, but all of them based around an oxygen plasma, resulted in the most reliable devices. Inclusion of the hole transport layer PEDOT-PSS was also successful over a wide range of literature, indicating that it too, with optimization, would ultimately improve device function. Attempts to reproduce results

seen by others, especially on novel and untried methods, such as the sodium hydroxide insulating layer, will not be a productive approach for the LED novice.

REFERENCES

1. Yang, Y.; Pei, Q. and Heeger, A. J. *J. Appl. Phys.* **1996**, *79*, 934.

2. Grice, A. W.; Bradley, D. D. C.; Bernius, M. T.; Inbasekaran, M.; Wu, W. W. and Woo, E. P. *Appl. Phys. Lett.* **1998**, *73*, 629.

3. Yan, H.; Huang, Q. L.; Cui, J.; Veinot, J. G. C.; Kern, M. M. and Marks, T. J. *Adv. Mater.* **2003**, *15*, 835.

4. Jakubiak, R.; Collison, C. J.; Wan, W. C.; Rothberg, L. J. and Hsieh, B. R. *J. Phys. Chem.* **1999**, *103*, 2394.

5. Brown, A. R.; Bradley, D. D. C.; Burroughes, J. H.; Friend, R. H.; Greenham, N. C.; Burn, P. L.; Holmes, A. B. and Kraft, A. *Appl. Phys. Lett.* **1992**, *61*, 2793.

6. Shi, Y.; Liu, J. and Yang, Y. *J. Appl. Phys.* **2000**, *87*, 4252.

7. Donley, C. L.; Zaumseil, J.; Andreasen, J. W.; Nielsen, M. M.; Sirringhaus, H.; Friend, R. H. and Kim, J-S. *J. Am. Chem. Soc.* **2005**, *127*, 12890.

8. Nguyen, T-Q.; Kwong, R. C.; Thompson, M. E. and Schwartz, B. J. *Appl. Phys. Lett.* **2000**, *76*, 2454.

9. You, Z. Z. and Dong, J. Y. *Vacuum* **2007**, *81*, 819.

10. Zhong, Z. Y. and Jiang, Y. D. *Phys. Status Solidi A* **2006**, *203*, 3882.

11. Han, I-M. and Hong, F. C-N. *Thin Solid Films* **2003**, *444*, 254

12. Crispin, X.; Jakobsson, F. L. E.; Crispin, A.; Grim, P. C. M.; Andersson, P.; Volodin, A.; Van Haesendonck, C.; Van der Auweraer, M.; Salaneck, W. R. and Berggren, M. *Chem. Mater.* **2006**, *18,* 4354.

13. De Jong, M. P.; van IJzendoorn, L. J. and de Voigt, M. J. A. *Appl. Phys. Lett.* **2000**, *77*, 2255.

14. Jin, Y.D.; Ding, X.B.; Reynaert, J.; Arkhipov, V.I.; Borghs, G.; Heremans, P.L. and Van der Auweraer, M. *Org. Elec.* **2004**, *5*, 271.

15. Zhu, F.; Low, B.; Zhang, K. and Chua, S. *Appl. Phys. Lett.* **2001**, *79*, 1205.

16. Schmitz, C.; Pösch, P.; Thelakkat, M.; Schmidt, H-W.; Montali, A.; Feldman, K.; Smith, P. and Weder, C. *Adv. Funct. Mater.* **2001**, *11*, 41.

17. Kim, J. S.; Granström, M.; Friend, R. H.; Johansson, N.; Salaneck, W. R.; Daik, R.; Feast, W. J. and Cacialli, F. *J. Appl. Phys.* **1998**, *84*, 6859.

18. Chan, I-M. and Hong, F. C-N. *Thin Solid Films* **2003**, *444*, 254.

19. Wu, C. C.; Wu, C. I.; Sturm, J. C. and Kahn, A. *Appl. Phys. Lett.* **1997**, *70*, 1348.

20. Wantza, G.; Hirsch, L.; Hubya, N.; Vignaua, L.; Silvainc, J.F.; Barrie´reb, A.S. and Parneix, J.P. *Thin Solid Films* **2005**, *485*, 247.

21. Liu, G.; Kerr, J. B. and Johnson, S. *Synth Met.* **2004**, *144*, 1.

22. Kim, K-B.; Tak, Y-H.; Han, Y-S.; Baik, K-H.; Yoon, M-H. and Lee, M-H. *Jpn. J. Appl. Phys.* **2003**, *42*, L438.

23. Choulis, S. A.; Choong, V-E.; Mathai, M. K. and So, F. *Appl. Phys. Lett.* **2005**, *87*, 113503.

24. Ashizawa, S.; Horikawa, R. and Okuzaki, H. *Synth. Met.* **2005**, *153*, 5.

25. Jabbour, G. E.; Kawabe, Y.; Shaheen, S. E.; Wang, J. F.; Morrell, M. M.; Kippelen, B. and Peyghambarian, N. *Appl. Phys. Lett.* **1997**, *71*, 1762.

26. Salaneck, W. R.; Stafström, S. and Bredas, J.-L. **Conj. Poly. Surface and Interfaces**, Cambridge University Press, Cambridge, 1996.

27. Montali, A.; Smith, P. and Weder, C. *Synth. Met.* **1998**, *97*, 123.

28. Hu, Y.; Shi, S.; Zhang, Y.; Zhou, Q.; Wang, L.; Ma, D. and Li, X. *Thin Solid Films* **2005**, *489*, 262.

29. Ma, L.; Xie, Z.; Liu, J.; Yang, J.; Cheng, Y.; Wang, L. and Wang, F. *Appl. Phys. Lett.* **2005**, *87*, 163502.

30. Wu, C-G. and Chang, S-S. *J. Phys. Chem. B* **2005**, *109*, 825.

31. Wantz, G.; Hirsch, L.; Huby, N.; Vignau, L.; Silvain, J. F.; Barriére, A. S. and Parneix, J.P. *Thin Solid Films* **2005**, *485*, 247.

32. Ishida, T.; Kobayashi, H. and Nakato, Y. *J. Appl. Phys.* **1993**, *73*, 4344.

33. Burrows, P. E.; Shen, Z.; Bulovic, V.; McCarty, D. M.; Forrest, S. R.; Cronin, J. A. and Thompson, M. E. *J. Appl. Phys.* **1996**, *79*, 7991.

APPENDIX

INITIAL STUDIES ON MIXED- POLYMER SOLAR CELLS

Mixed polymer photovoltaics (PVs) based on polyfluorene copolymers F8BT, [poly(9,9'-dioctylfluorene-co-benzothiadiazole)], an excellent electron transport material and PFB, [poly(9,9'-dioctylfluorene-co-bis-N,N'-(4-butylphenyl)-bis-N,N'-phenyl-1,4-phenylenediamine)], an excellent hole transport material, have initially shown promise as a new generation of all polymer solar cells, with device efficiencies comparable to organic-based solar cells.[1-5] Polymer-based photovoltaics use the same configuration as diagrammed for the light emitting device, with the polymer mixture sandwiched between the two electrodes. The electron and hole transporting polymers are blended in order to create efficient exciton dissociation; the excitons formed can diffuse to a boundary between the two polymer materials and separate into the charges at borders between the two types of polymers- with electrons preferring the F8BT, and holes preferring the PFB.[1] These separated charges are then transported through their respective polymers to the desired electrode to produce current. Film morphology, important to the function of LEDs, is of vital importance in these blended polymer photovoltaics, since the two polymers phase segregate into domains that are not purely one polymer or the other, but instead produce mixtures that are a majority of one of the polymers, with smaller domains of the other polymer finely dispersed within the dominant polymer.[5-7] It has been shown through different spectroscopic examinations that the domains are predominately F8BT in the higher topographical areas seen in AFM scans, and the low-lying “holes” seen are predominately PFB.[1-7] There is an example of this morphology is shown in Figure A.1.

How well the PVs will work depends on exciton formation in the polymer film, combined with the degree of dissociation and transport of the charges to the electrodes. Similar to LEDs, charge injection into the electrodes faces a similar barrier as that from the electrodes, and improvements to the device were made by including a thin layer of PEDOT-PSS included along with a calcium/aluminum cathode.[8] Exciton formation is not a problem in the conjugated polymers, and similar to other CPs used in LEDs, excitons on polymer chains formed through light absorption tend to recombine and result in light emission, limiting the amount of dissociation.

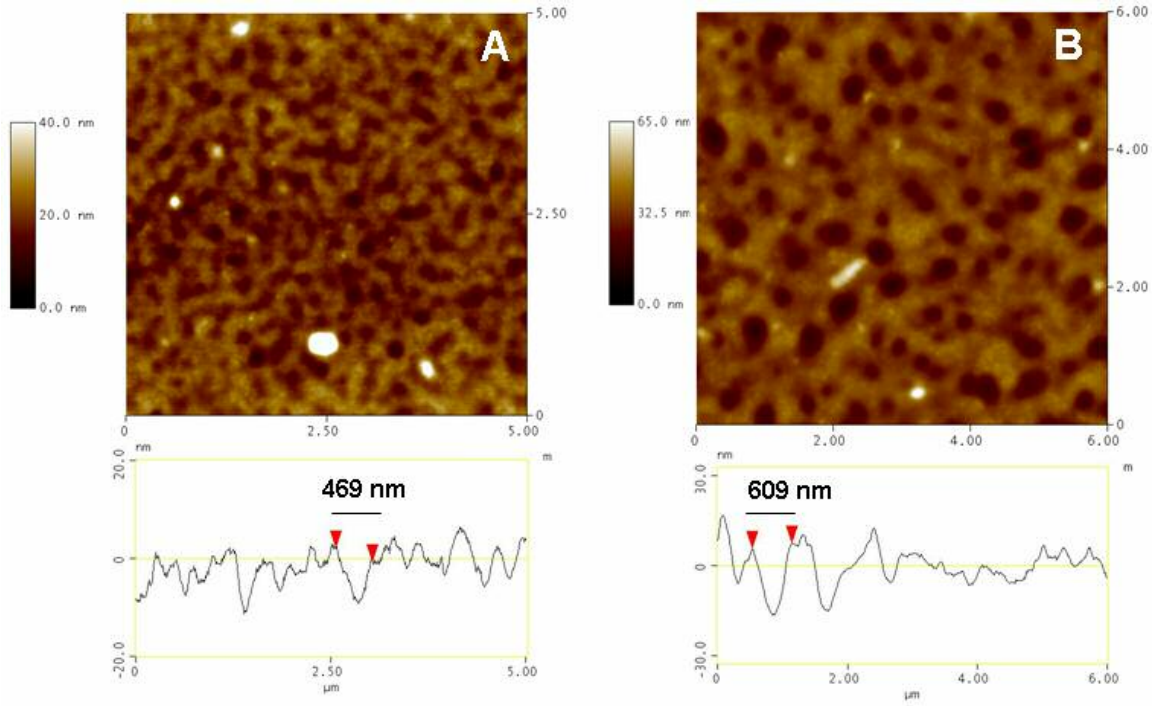

Figure A.1 AFM topography scans of 1:1 mix (15mg/mL) F8BT and PFB, in o-xylene (A) and p-xylene (B), showing the width of the low-lying PFB domains.

Since the exciton diffusion length is usually on the scale of ten nanometers for most organic semiconductors,[9-10] the domains rich in either polymer should ideally be on a similar size scale in order to break apart excitons the most efficiently; however, the separated charges then need to be carried along the polymer towards the electrodes and if these polymer domains are too small, the charges will likely encounter opposite charges, resulting in recombination and light emission.

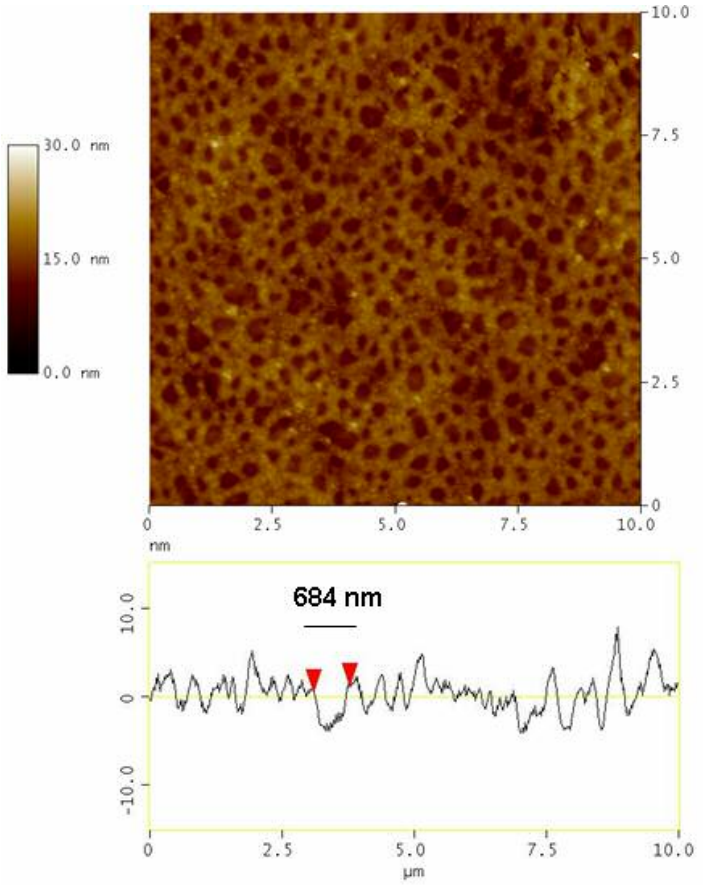

Figure A.2 AFM topography of a F8BT:PFB film thermally annealed in a saturated p-xylene environment, showing a smoother film with a slight increase in domain size.

Charge formation and transport are the two main factors contributing to device efficiency in PVs, and it is poorly understood exactly how much of either occurs, or to what degree they occur at different areas within the domains. The surface morphology of these films have been examined on the nanoscale using NSOM[1,5,8,12] and scanning Kelvin probe microscopy (SKPM)[11] to compare surface morphology to current generation. The results of these experiments have been directly opposed to one another; with the SKPM images indicating that the greatest amount of current was produced along the edges of domains, while the NSOM experiment, using the tip to locally excite a working PV, determined the highest current was in the center of the low-lying domains.

F8BT and PFB used in these studies were purchased from American Dye Source, used without further preparation. Duplicating the results seen by others[1-6] was initially attempted, by combining equal volumes of 15 mg/mL solutions of each polymer in o-xylene or p-xylene, then spincasting the solution mixture onto clean substrates. The xylenes are considered a poor solvent for the two polymers, thus films made from these polymers form large, well defined domains. Two AFM topography images of the films produced from o-xylene (A) and p-xylene (B) are shown in Figure A.1, along with their associated line scans indicating the width of the average PFB domains. Domains seen for F8BT:PFB films in the studies mentioned were on the length scale of a couple of microns; unfortunately, the domains seen in Figure A.1 are considerably smaller, with the larger sizes on the scale of ~ 600 nm diameter, this is sufficient for NSOM studies, but there was some curiosity as to why the films were different from what had been seen in the literature. The large white spots on the films are from undissolved polymer, which was filtered out from later AFM scans using a 100 nm filter, producing an identical film topography only without the high white spots. Attempts were then made to increase the

size of the polymer domains, initially by slowing the spincasting speed to control evaporation rates; which did produce large domains but also films too thick for use in PVs; then through thermal annealing of the films in a solvent-saturated environment. The result of the latter experiments produced varied results, with an example shown in Figure A.2, of a mixed polymer film that has been annealed at 100 ˚C for two hours in a saturated p-xylene atmosphere. This produced a very smooth topography with well-formed, but still not particularly large domains. Different solvents were examined, including toluene and chloroform, which led to interesting morphologies but often without the micron-scale domains. Spincasting films in a solvent saturated environment were also performed; these films did not show larger domains. Of the varied trials performed on the F8BT:PFB samples, only the slow spin speeds increased domain size to a significant degree, but the thickness of the films prevented further experiments. The discrepancies between the domain sizes shown in Figure A.1 and what had been presented in the literature were determined to be from the different molecular weights of the polymers used; the micron scale domains were produced using polymers made by Friend's group,[1-6,10,11] with a M_n of 112 kg/mol for F8BT, and 60 kg/mol for PFB, with a higher degree of crystallinity compared to the ADS polymers with a M_n of 30 kg/mol for F8BT and 20 kg/mol for PFB. Rather than continue trying to reproduce the larger domain sizes, the films prepared from p-xylene (with its slightly larger domain sizes) were used for further studies.

Currently, sandwich-type photovoltaic devices made from the F8BT:PFB mixture are undergoing similar photocurrent measurements as to what has already been shown,[8] but with higher resolution, being examined by David Ostrowski. Photocurrent measurements will then be combined with NSOM fluorescence lifetime imaging experiments, taken by Catherine Kitts, from which the areas where the greatest amount of

exciton dissociation is occurring can be determined, as these areas will produce shorter lifetimes compared to areas where only a small amount of excitons are dissociating. The combination of the two will provide insight on where the greatest amount of excitons are dissociating, as well as where the separated charges are transported the most efficiently; since it is unknown whether the device is limited by charge dissociation or charge transport within these films. Preliminary results on lifetime imaging indicate that the there are no dramatic differences in lifetimes along the film, but the shortest lifetimes are seen along the edges of the low-lying domains (rich in F8BT), indicating that excitons dissociate fairly evenly over the film, with the greatest amount of dissociation occurring at the boundaries of the polymer domains. Successful photocurrent measurements are still ongoing.

SUMMARY

Understanding how charges move within conjugated polymer films is of great importance to these semiconducting films used in LEDs, and is of vital importance in mixed polymer photovoltaics. These films are very complex systems, with more than just charge transport affecting device efficiencies, and studying these interactions can only be done indirectly, with the effects inferred from the data produced. Through the application of scanning probe methods that can measure optical and physical information on the nanoscale, such as NSOM and AFM, data from these films can be combined with the knowledge gained from studying charge transport within single homopolymer systems in conjugated polymer films used for LEDs, will allow for better understanding of how charges move within different films, and how to increase desired charge movements to improve device efficiencies.

REFERENCES

1. Arias, A. C.; MacKenzie, J. D.; Stevenson, R.; Halls, J. J. M.; Inbasekaran, M.; Woo, E. P.; Richards, D. and Friend, R. H. *Macromolecules* **2001**, *34*, 6005.

2. Halls, J. J. M.; Arias, A. C.; MacKenzie, J. D.; Wu, W.; Inbasekaran, M.; Woo, E. P. and Friend, R. H. *Adv. Mater.* **2000**, *12*, 498.

3. Coffey, D. C. and Ginger, D. S. *Nature Mat.* **2006**, *5*, 735.

4. Snaith, H. J. and Friend, R. H. *Thin Solid Films* **2004**, *451*, 567.

5. Milner, R. G.; Arias, A. C.; Stevenson, R.; MacKenzie, J. D.; Richards, D.; Friend, R. H.; Kang, D.-J.; Blamire, M. *Mater. Sci. Technol.* **2002**, *18*, 759.

6. Kim, J-S.; Ho, P. K. H.; Murphy, C. E. and Friend, R. H. *Macromolecules* **2004**, *37*, 2861.

7. Stevenson, R.; Arias, A. C.; Ramsdale, C.; MacKenzie, J. D. and Richards, D. *Appl. Phys. Lett.* 2001, *79*, 2178.

8. McNeill, C. R.; Frohne, H.; Holdsworth, J. L. and Dastoor, P. C. *Nano Lett.* **2004**, *4*, 2503.

9. Haugeneder, A.; Neges, M.; Kallinger, C.; Spirkl, W.; Lemmer, U.; Feldmann, J.; Scherf, U.; Harth, E.; Gügel, A. and Müllen, K. *Phys. Rev. B* **1999**, *23*, 15346.

10. Markov, D. E.; Amsterdam, E.; Blom, P. W. M.; Sieval, A. B. and Hummelen, J. C. *J. Phys. Chem. A* **2005,** *109,* 5266.

11. Chiesa, M.; Bürgi, L.; Kim, J-S.; Shikler, R.; Friend, R. H. and Sirringhaus, H. *Nano Lett.* **2005**, *5*, 559.

12. Riehn, R.; Stevenson, R.; Richards, D.; Kang, D-J.; Blamire, M.; Downes, A. and Cacialli, F. *Adv. Funct. Mater.* **2006**, *16*, 469.

Vita

Lynn June Rozanski was born in Myrtle Beach, SC on February 24, 1980 to Margy Hougland and Richard R. Rozanski. She spent most of her childhood living in southern Arizona and spending summers in Florida. She graduated from Buena High School in Sierra Vista, AZ in May of 1998 and received her Bachelors of Science in Chemistry from the University of Arizona, in Tucson, AZ in May of 2002. After graduation, she moved to Austin, Texas to pursue her PhD in Analytical Chemistry and Nanotechnology Portfolio under the supervision of Dr. David A. Vanden Bout.

Permanent address: 6681 E Kendall Lane, Sierra Vista, AZ, 85650

This dissertation was typed by Lynn Rozanski.